GE Nuclear Energy

GE Nuclear Energy

General Electric Company
175 Curtner Avenue, San Jose, CA 95125

NEDC-32301
Revision 0
Draft
Class 2
December 1993

Single Tube Condensation Test Program

W. R. Usry

Reviewed: _____
T. R. McIntyre, Manager
Testing & Performance Analysis
SBWR Project

Approved: _____
P. W. Marriott, Manager
SBWR Project

DISCLAIMER OF RESPONSIBILITY

This document was prepared by the General Electric Company (GE). No other use, direct or indirect, of the document or the information it contains is authorized; and with respect to any unauthorized use, GE does not make any representation or warranty (express or implied) as to the completeness, accuracy, or usefulness of the information contained in this document or that such use of such information may not infringe privately owned rights; nor does GE assume any responsibility for liability or damage of any kind which may result from such use of such information. Furnishing this document does not convey any license, express or implied, to use any patented invention or any information of GE disclosed herein, or any rights to publish the document without prior written permission of GE.

ABSTRACT

An experimental program was conducted to investigate steam condensation inside of tubes in the presence of noncondensables. The work was conducted at UC Berkeley and at MIT. The work was initiated in order to obtain a database and a correlation for heat transfer in similar conditions as would occur in the SBWR PCCS tubes during a DBA LOCA. Three researchers utilized three separate experimental configurations at UC Berkeley while two researchers utilized one configuration at MIT. The researchers ran tests with pure steam, steam/air, and steam/helium with flowrates and noncondensable mass fractions representative and bounding of a DBA LOCA. The experimenters found the system to be well behaved for all tests with either of the noncondensables for forced flow conditions similar to the SBWR design. The results of the first test at UC Berkeley became the basis for the correlation used currently in the computer code TRACG. Recent tests at UC Berkeley have shown that the version of the correlation installed in TRACG generally overpredicts the gas-side heat transfer. A correlation based on the latest Berkeley data was used to show that the latest data do not significantly impact the containment performance.

ACKNOWLEDGMENTS

The single tube condensation tests were conducted by students and staff at the University of California at Berkeley and at MIT. The author has learned much from his interactions with Professors Schrock and Golay. Their efforts in assisting with the preparation of this report, which will support SBWR design certification in the U.S., have been invaluable. In addition, the efforts of Joseph Kuhn and Professor P. Peterson to help meet the deadline of this report are appreciated. The reviews and subsequent comments by Jim Fitch and Jens Andersen were invaluable and are also appreciated.

TABLE OF CONTENTS

NOMENCLATURE

Symbol	Description
b	constant
C	constant
c_p	specific heat at constant pressure
D	Diameter (no subscript indicates inner diameter)
f	degradation factor
f_R	friction factor
g	gravity force
h	heat transfer coefficient
h_{fg}	latent heat of vaporization
h_{fg}'	modified latent heat of vaporization
HP	horsepower
ID	inside diameter
Ja	Jakob number = $Cp_m/(T_b-T_w)/h_{fg}$
k	thermal conductivity
L	length
M_a	noncondensable gas mass fraction
MIT	Massachusetts Institute of Technology
N	number of data points
Nu	Nusselt number = hD/k_m
OD	outside diameter
P	pressure
q"(x)	local heat flux as a function of x
R	thermal resistance
Re	Reynolds number (defined in text)
s	standard deviation
T	temperature
U	velocity
UCB	University of California at Berkeley
W	mass flow rate
x	axial coordinate along condensing surface referenced to the top
X	mole fraction
z	axial coordinate in the coolant annulus

Greek Letters	
δ_1	condensate film thickness assuming no interfacial shear
δ_2	condensate film thickness assuming interfacial shear
Γ	condensate mass flow rate per unit width
τ	shear
ρ	mass density
μ	viscosity
ν	kinematic viscosity = μ/ρ
ϕ	function

Subscripts

a	air or other noncondensable
a	adiabatic wall
b	bulk
c	coolant
Cw	Cooling water
eff	effective
exp	from experiment
f	film
g	gas
i	inner or interface
in	inlet
l	liquid
m	mixture
o	outer
ref	reference
sat	saturation
t	turbulent
v	vapor
w or W	wall
Win	inner wall
Wo	outer wall

LIST OF TABLES

LIST OF FIGURES

1. INTRODUCTION

Investigations by the University of California at Berkeley (UCB) and by Massachusetts Institute of Technology (MIT) have been conducted in order to experimentally investigate thermal-hydraulic conditions similar to those that will occur in the SBWR passive containment cooling system (PCCS) tubes. A correlation of the data is used in the code TRACG to help predict the performance of the SBWR PCCS system. This report describes and summarizes the test programs and their results to date. Reporting details of data and the various apparatus is not within the scope of this report. That information is best described first hand by the original authors Vierow [1990], Vierow and Schrock [1991], Siddique [1992], Ogg [1991], Schrock et al. [1994], and Kuhn et al. [1993]. This report summarizes results of each of the programs with reference to the SBWR design and in light of the increased knowledge available at the writing of this report.

1.1 Background

The PCCS is a post-LOCA, low pressure, decay heat removal system of the SBWR as described in Wilkins et al. [1992] and Vierow et al. [1992]. It is designed to remove decay heat from the containment and maintain pressure and temperature at or below design limits for a minimum of 3 days. A large volume suppression pool absorbs the energy released in the initial blowdown phase and limits the initial containment pressure rise. The PCCS tubes remove essentially all of the decay heat during the long-term phase.

The PCCS tubes act as the heat exchanger for the PCCS. They are located in a large pool of water outside the containment boundary and represent an extension of the boundary. The PCCS tube receives a steam and noncondensable gas mixture from the drywell and condenses the steam. The condensate flows down to a Gravity Driven Cooling System (GDCS) pool while the remaining gas flow is vented to the suppression pool. The gas flow to the heat exchanger is driven by the combined effects of condensation and the pressure difference between the drywell and the suppression pool pressure at the depth of the vent line (0.75 m nominally). Thus, in general, the flow through the tubes is forced flow and not natural circulation driven.

1.2 Necessity of Test Program

The PCCS tubes are an essential part of the SBWR passive heat removal systems. In order to develop and qualify modeling tools which evaluate the performance of the overall system, experimental data are needed. Before the initiation of this investigation, experimental data for steam condensation inside of tubes in the presence of noncondensables were rare. The data that were available only showed average heat transfer results. To make appropriate use of detailed thermal-hydraulic codes, such as TRACG, requires correlation of local heat transfer data. An understanding of steam condensation in the presence of noncondensables necessitates that local quantities such as noncondensable mass fractions, local condensate flow rate, and local heat flux be resolved.

1.3 Scope of Testing

The intent of this experimental program was to obtain a base of local heat transfer data for the range of steam/noncondensable flows expected in a DBA LOCA. This database has been used to develop a correlation suitable to TRACG and other codes and to support the evaluation of post-LOCA performance of the SBWR containment. The tubes used in the tests were prototypical in size, with the exception of the initial test at UC Berkeley which had a 1 inch diameter tube instead of a 2 inch diameter tube.

The noncondensable gas that would be present in a DBA LOCA would be essentially all nitrogen from the inert containment atmosphere (negligible quantities of hydrogen and oxygen are produced by radiolysis). Under severe accident conditions hydrogen may be produced by a steam-zircaloy reaction. For safety reasons and for experimental ease, these noncondensables were represented by air and helium, respectively. Air and helium have similar properties to nitrogen and hydrogen, respectively, and are expected to closely mimic the effects of nitrogen and hydrogen on the condensation process. The pressure range for the experiments was from 0.3 to 5 atmospheres. The steam flowrates ranged from 20 to 60 kg/hr. The air inlet mass fractions ranged from 0 to 0.40 while the helium mass fractions ranged from 0 to 0.20. The cooling side of the heat exchanger was accomplished by forced convection of subcooled water.

1.4 Status of Test Program

The tests being conducted at UC Berkeley and MIT were scheduled to be completed in October of 1993. This report was intended to be the final report on the subject. However, both Universities experienced delays, largely caused by equipment failures. Both Universities are finished taking data and are in the process of reducing and analyzing the data. UC Berkeley will issue a final report in January of 1994 and MIT will issue a report on their current work in the first half of calendar 1994. This present report includes much of the results of the latest UC Berkeley work. After the universities complete their work, GE will submit the final report on the single tube condensation tests.

2. TESTS

Three separate series of tests were conducted at UC Berkeley and two series of tests were conducted at MIT. What follows in this chapter summarizes the equipment and the results of these tests. A more detailed discussion may be found in the appropriate references (Vierow [1990], Vierow and Schrock [1991], Siddique [1992], Ogg [1991], Schrock et al. [1994] and Kuhn et al. [1993]).

2.1 Vierow (UC Berkeley)

The first test program was performed by K.M. Vierow at UC Berkeley. The experiment utilized a natural circulation loop with a 1 inch diameter copper condensing tube. Detailed documentation and results may be found in Vierow [1990] and Vierow and Schrock [1991].

2.1.1 Apparatus

The experimental facility had the following basic components: pressure vessel/boiler, steam inlet lines; lower plenum; riser; condensing test section; condensate drain system; and instrumentation. Figure 2.1-1 shows a schematic of the system and Figure 2.1-2 illustrates the instrumentation. With the exception of the drain line, all components were insulated in order to minimize heat loss. The body of the electrically heated boiler was a 2.74 m long, 0.305 m IPS (International Pipe Standard) Schedule 5 stainless steel pipe. A 0.305 m IPS Schedule 10 pipe cap was welded to the top and the bottom. A blowdown line consisted of a 1.27 cm outside diameter (OD) stainless steel tube that led to a water-filled reservoir. The pressure relief valve was set to open at 100 psig. The air intake line was taken off the blowdown line, upsteam of the relief valve.

Three immersion heaters were installed through a 6.4 cm coupling at the bottom of the pressure vessel. The heaters were 1 cm OD stainless steel, sheathed Calrod type heaters. The heaters were able to produce a combined power level greater than 20 kW which was the maximum power used in this experiment. Steam was carried from the boiler to the lower plenum by a 2.54 cm OD stainless steel tube. The lower plenum was used to mix steam with air before entering the test section. The steam/air mixture exited the plenum and entered a riser made of 5.08 cm tube, 2.41 m in length. The mixture then passed through two 90° bends and entered the condensing test section. The test section consisted of a double-pipe, concentric-tube heat exchanger. The inner tube through which

the steam/air mixture flowed was a 2.21 cm ID, 2.54 cm OD copper tube of length 2.39 m, 0.25 m of which was not available for condensation. The condensate and the noncondensables exited the test section into the lower plenum through the downcomer. The condensate flowed out through a double-pipe, concentric-tube heat exchanger and into a graduated cylinder. The noncondensables were recirculated with incoming steam back through the test section.

The cooling jacket was constructed of four 0.483 m sections of 5.08 cm stainless steel tubes flanged together. The flanges extend out from the tube on both the inside and the outside. The outside sections were bolted together. The inside sections of the three pairs of flanges had a 2.59 cm inner diameter to allow the flanges to just slide over the condenser tube. Each side of the flange pairs had 12 0.715 cm diameter holes spaced equally around the flange. The flange pairs were separated by a small distance and the holes were intentionally misaligned in order to promote mixing. The cooling water entered the bottom of the cooling annulus through custom-made heat exchanger fittings and exited at the top. The coolant flow rate was controlled to provide nearly complete steam condensation and also maintain a coolant temperature rise sufficient to determine local heat transfer rates.

All thermocouples were copper-constantan (T-type) except for six iron-constantan (J-type) in the boiler. The thermocouples used to measure fluid temperatures were 24-gauge, 0.159 cm OD, stainless steel Omega probes mounted through CONAX gland fittings sealed with Teflon disks. Nine thermocouples were mounted on the condenser tube outer wall. Three thermocouples measured the temperature in the cooling annulus after each of the three flange pairs. These three thermocouples plus thermocouples in the coolant water inlet and outlet combined for a total of five coolant water measurements. Pressure transducers were located in the lower plenum and at the top of the loop as shown in Figure 2.1-2.

In each of the experiments at the two universities, the calculation of the local heat transfer coefficients was done in a similar manner. The local heat transfer coefficient is defined as:

$$h(x) = q''(x) / (T_{sat}(x) - T_w(x)) \qquad 2.1\text{-}1$$

where $T_w(x)$ is the temperature of the inner wall of the condensing tube, $T_{sat}(x)$ is the local (in the axial dimension only) saturation temperature of the steam/air mixture, and x is referenced to the top of the condensing section. The local heat flux, q"(x), is found from:

$$q''(x) = -\frac{W_c c_p}{\pi D_i}\frac{dT_b(x)}{dx} \qquad 2.1\text{-}2$$

where $T_b(x)$ is the bulk temperature of the cooling water at an axial location, W_c is the coolant mass flow rate and c_p is the specific heat at constant pressure of the coolant. The temperature $T_{sat}(x)$ is not measured directly but must be determined by knowledge of the amount of steam that has condensed. The mass flow rate of the noncondensable remains constant along the length of the tube. The steam mass flow rate decreases because steam is condensed. Thus, if the amount of steam condensed can be determined then the partial pressure of the steam (and therefore the saturation temperature) is known as a function of axial position. This assumes that the total pressure remains constant along the length of the tube. This is a valid assumption because the pressure drop through the condensing section is very small. (A friction factor of 0.025 produces a pressure drop of 75 Pa for run 1.1-1 of Kuhn. Data shown in Appendix). The condensate mass flow rate as a function of axial distance is:

$$W_i(x) = \frac{W_c c_p (T_b(0) - T_b(x))}{h'_{fg}} \qquad 2.1\text{-}3$$

where h'_{fg} is a corrected form of the heat of vaporization, h_{fg}, to account for condensate subcooling.

$$h'_{fg} = h_{fg} + \text{Constant} \cdot c_p(T_{sat} - T_w) \qquad 2.1\text{-}4$$

The Constant quoted in textbooks and literature ranges from 3/8 to 0.68 and different constants were used with different experiments. The sensitivity of the results to the value of the Constant is small because the heat of vaporization is large compared with the correction part of the equation. The inner tube wall temperature is computed by a conduction correction from the outer wall temperature. The partial pressure of the steam is now easily determined which then specifies T_{sat}. Thus, h(x) can now be calculated.

2.1.2 Discussion of Results

Vierow ran a total of 35 tests. In 18 of those tests the system reached a steady state and the condenser tube wall temperature monotonically decreased with distance from the entrance to the condensing section. In 12 tests which reached a steady state the condenser tube wall temperature increased with distance from the entrance and then between 24 and 48 cm downsteam the temperature monotonically decreased to the cooling water temperature. This was termed a "temperature inversion" and was an unexpected finding. Typical plots of cases with and without temperature inversions are shown in Figure 2.1-3. Temperature inversions occurred when the air mass fraction was low and were more in evidence as the heater power was increased. In three cases system oscillations occurred during startup with the system settling to a steady state and in two cases oscillations occurred which did not die out. Both of these took place when the air content was high.

The flow oscillations are described in both Vierow [1990] and Vierow and Schrock [1991]. Plots of tube wall and coolant outlet temperature with time are shown in Figure 2.1-4. While the flow oscillations are phenomenologically interesting, they are not applicable to the SBWR PCCS design. The Vierow experiment was a pure natural circulation driven flow, i.e. flow ceases when heat transfer ceases. The SBWR PCCS tube flow is forced circulation driven by the pressure difference between the drywell and the wetwell, even for small inlet noncondensable mass fractions.

The non-oscillatory runs from Vierow can be divided into those with temperature inversions and those without. A partial explanation of the temperature inversions are made in Vierow [1990] starting on page 59. Siddique at MIT [1992] and the latest tests at UCB, Kuhn et al. [1993], both forced circulation experiments, do not report the existence of such a temperature inversion. Schrock [1993] postulates that it is a result of the setup of the flow in a manner which appears to be unique to natural circulation. The data from runs with a temperature inversion were not included in the Vierow-Schrock correlation ("Tsukuba" correlation), discussed in Section 3.1, on the above-mentioned basis that they are inapplicable to the SBWR with its forced venting mechanism

2.1.3 Experimental Uncertainties

The two most prominent uncertainties in this experiment were: 1) determining the inlet air mass fraction, 2) determining the coolant bulk temperature. In order to obtain the air mass fraction at the condenser entrance, the air holdup was determined from

approximate calculations as explained in Vierow [1990]. This likely contributes to the data scatter shown in Section 3.1. There is also some uncertainty in the determination of the coolant bulk temperature from the available temperature measurements. The procedure relies on the flow becoming well-mixed due to the fluid having to flow through pairs of flanges with non-aligned holes. One helpful bit of knowledge gained from this experiment was insight on the shape of the heat flux curve. As a result subsequent UCB tests used a nonuniform thermocouple spacing with measurements concentrated near the entrance where most of the condensation occurs.

2.2 Siddique (MIT)

Siddique at MIT also investigated steam condensation inside tubes in the presence of noncondensables. He utilized a forced flow system with a 2 inch diameter condensing tube. Detailed documentation and results may be found in Siddique [1992].

2.2.1 Apparatus

The experimental facility has the following basic components: pressure vessel/boiler, steam inlet lines, condensing test section, condensate drain system, throttle valve, and instrumentation. Figure 2.2-1 shows a schematic of the whole system and Figure 2.2-2 illustrates the test section. The electrically heated boiler was a cylindrical stainless steel vessel 4.5 m high by 0.45 m inside diameter. Power was supplied by four immersion type sheathed electrical heaters, each nominally rated at 7 kilowatts. A high precision wattmeter measured the power input to the boiler. The noncondensables were supplied to the base of the boiler through a pressure regulating valve, a calibrated rotameter, and a flow control valve. Mixing of the steam with the noncondensable gas was achieved in the boiler vessel. The steam/gas mixture left the vessel through an isolation valve located near the top of the vessel. The mixture temperature, pressure and flowrate were measured before entering the test section. The condenser tube was a stainless steel tube with an OD of 50.8 mm and an ID of 46.0 mm and 2.54 m in effective length. Condensate was collected in the condensate separator/collector drum. The noncondensable gas and the uncondensed steam, if any, were vented from this drum to the to the atmosphere via a throttle valve. The cooling jacket was constructed of 62.7 mm inside diameter stainless steel tubing. As in Vierow, the cooling water flowed upward through the annulus while the steam/noncondensable mixture flowed downward through the condensing tube. The cooling water was pumped through the test section and then to a drain after passing through a rotameter and a flow control valve. To prevent thermal

stresses, a sliding O ring joint at the lower end of the condenser was used to allow relative movement between the condenser tube and the cooling jacket tube.

All thermocouples were iron-constantan (J-type). Temperature measurements were made of the inside and outside condensing tube wall temperature and of the cooling water at nine locations spaced 30.5 cm apart along the length of the condenser. Temperature measurements of the gas mixture were also made along the centerline of the condenser, but were not used in the data reduction. The inner wall thermocouples were 0.8 mm OD SS sheathed probes that were embedded in drilled holes filled with silver solder. The holes entered the tube wall at an angle and were drilled so as to locate the junction of the thermocouple at less than 0.2 mm from the inner surface of the tube wall. The outer wall thermocouples were the same type of probes as the inner wall probes and were each embedded in a longitudinally machined groove with the dimensions 0.9 mm wide by 0.4 mm deep and 12.7 mm in length. The hole was brazed with silver solder. All of the tube wall thermocouple leads entered the test section at the top and were strung through the cooling jacket annulus to the axial location for that particular thermocouple. Details of the thermocouple locations are shown in Figure 2.2-3.

The cooling water temperature measurements were made using a 1.6 mm OD SS sheathed rigid thermocouple probe that was inserted through the cooling jacket as shown in Figure 2.2-3. In order to get an accurate measure of the bulk coolant temperature good mixing was required in the annulus. The easiest way of accomplishing this is to supply cooling water at a rate so that the flow is turbulent within the annulus. However, for this configuration the flowrates required would not have allowed a sufficiently large temperature difference between the inlet and outlet coolant flow water. Siddique's solution to this was to bubble in small amounts of air through the annulus so that good mixing could be accomplished while achieving a large enough coolant water temperature rise. Siddique did not specify the amount of air which was added to the water. Measurements of the inlet and outlet cooling water temperature were also made.

The data reduction methods used by Siddique are similar to those used by Vierow and were explained in Section 2.1.1. Thermocouples located on both the inside and the outside of the condenser tube wall were intended to be a redundant method of obtaining the heat flux through the wall. However, large scatter in the tube outer wall temperature measurements occurred and the method was abandoned.

2.2.2 Discussion of Results

Siddique ran 52 air/steam and 22 helium/steam tests. He reported neither oscillations in the test experiment nor a temperature inversion. His inlet air mass fractions ranged from 0.09 to 0.42. A test matrix is shown in Table 2.2-1.

Comparison of heat transfer coefficients of Siddique and those produced from the correlation in Vierow [1990] are shown in Figure 2.2-4. **Note that the correlation used for comparing the UCB data is not the "Tsukuba" correlation of Vierow and Schrock [1991], but is an unpublished correlation from Vierow's thesis.** Notwithstanding, it is still useful for this comparison. It is clear from both plots that the MIT data predict much higher heat transfer coefficients than does the correlation in Vierow [1990]. This will be explored in more detail in Section 2.2.3.

Siddique tested helium/steam mixtures as well as air/steam mixtures. He reported that, for the same mass fraction, helium degrades the heat transfer more than air does. For the same mole fraction, air degrades the heat transfer more than does helium. This is a useful, but not a surprising result. The gas-side heat transfer is controlled to a large extent by the partial pressure of steam near the condensate/gas interface. The lower the partial pressure of steam is (for a given total pressure) the lower the heat transfer will be. The partial pressure of steam *at the interface* is controlled by the partial pressure (or equivalently volume fraction and therefore mole fraction) of the noncondensable gas *at the interface*. This, in turn, is controlled by two factors: the *bulk* amount of the noncondensable gas in moles and its ability to diffuse away from the interface. Because helium has near an order of magnitude greater moles per unit mass than does air, one would expect it to degrade the heat transfer more than air does on a mass basis. As steam condenses, a concentration gradient of noncondensable gas appears near the condensate/gas mixture interface. The ability of the noncondensable to diffuse in steam will then determine the partial pressure of the noncondensable at the interface for a given bulk molar fraction. Therefore, a gas that diffuses well in steam will degrade steam condensation heat transfer less than a gas that diffuses poorly. Helium diffuses much better than air in steam and as a result does not degrade heat transfer as much as air does on a molar basis.

Plots comparing the ratio of Nusselt numbers of the system run with helium and the system run with air are shown in Figure 2.2-5 and 2.2-6. Siddique did not experience

any differences running the system with helium versus air. No unusual profiles, no transients, and no stalling were reported.

2.2.3 Experimental Uncertainties

Data from the current tests at MIT (not presented in this report) as well as analysis of Siddique's data at UCB reveal some questions about the data reduction which resulted in large heat transfer coefficients near the entrance of the tube. In analyzing the data for the Vial correlation (Section 3.4), UCB discovered that Siddique extrapolated the coolant temperature at the upper end of the test section. The first cooling jacket thermocouple was located at a distance of 41 cm from the entrance of the tube. Siddique reported condenser tube wall temperatures at a distance of 10 cm from the inlet but did not report a coolant water temperature. He took the bulk temperature of the coolant at $x = 0$ to be the value recorded by the thermocouple located on the coolant exit pipe. It was not clear that this was indeed measuring the bulk temperature of the coolant. Trying to fit a coolant temperature curve for $x < 41$ cm using the coolant exit temperature was difficult to justify and thus only the data at locations greater than or equal to $x = 41$ cm were included in the Vial correlation. Golay [1993] agreed to this treatment of the data. With this data excluded the large differences in heat transfer near the entrance of the tube, shown in Figure 2.2-4, are eliminated. Possible additional sources of error not reported by Siddique are: 1) uncertainties in obtaining the bulk coolant temperature measurements and 2) design problem associated with the coolant flow outlet.

Siddique's method of injecting air bubbles into the coolant to promote turbulence is a reasonable procedure but the documentation of the experiments does not provide sufficient detail for a complete evaluation. A detailed evaluation is included in the current MIT experiment. Another possible concern about obtaining the bulk coolant measurements is that all the thermocouple leads for the condenser tube wall are led up through the annulus and exit at the top. This is a problem which is difficult to avoid, but nevertheless, the leads can potentially disturb the flow and possibly cause stagnant regions near the condenser tube.

Figure 2.2-7 shows detail of the test section upper end. The figure shows that there is a region above the coolant outlet where cooling may take place. An improved design would have the coolant outlet flush with the top end of the available condensing tube. The problem is compounded by the possibility that air may air collect at the top of the coolant annulus and inhibit heat transfer. Also like Vierow, the coolant outlet is

located at only one circumferential location. This could affect the coolant hydrodynamics near the coolant outlet (and inlet) resulting in erroneous bulk temperature measurements.

2.3 Ogg (UCB)

Ogg at UC Berkeley utilized a forced flow system with a 2 inch diameter condensing tube. Detailed documentation and results may be found in Ogg [1992].

2.3.1 Apparatus

The apparatus in Ogg's experiment consisted of a campus steam supply system, a gas supply system, test section, separator, cooling water system, piping, and instrumentation and data acquisition system. A schematic of the overall system is shown in Figure 2.3-1. The steam was supplied by the 120 psig UC Berkeley campus steam system. Air was supplied by a 100 psig building air supply and the Helium was supplied from high pressure cylinders. Both the steam and the noncondensable gas each flowed through separate 2.54 cm IPS lines with metering sections for both high flow rates for low flow rates. Downstream of the metering sections the gas and the vapor were mixed and were delivered to the test section.

The condensing tube was a 3.5 m long 5.08 cm 321 stainless steel tube with a 0.071 cm wall thickness. To provide an adiabatic entrance length the top 0.787 m was insulated. The bottom 0.278 m of the tube was also not available for condensation which left 2.44 m for the active length. Like Vierow and Siddique, forced convection cooling water flowed upward in the annular space between the condensing tube and a cooling water jacket. This jacket was constructed from five sections of 6.35 cm OD stainless steel tubing with a 0.305 cm wall thickness. These sections were flanged together in a similar manner as Vierow. The flanges formed mixers which were just upstream of a cooling water thermocouple. An outlet plenum mounted at the bottom of the test section directed the condensate, the noncondensable gas and any uncondensed steam to the separator. Separation of the condensate from the gas phase was accomplished with a 1.27 cm Armstrong float trap which only allowed liquid to pass. Measuring the condensate flow rate served as a check of the steam metering system.

A 3/4 HP centrifugal Grundfos pump supplied the cooling water to the cooling water jacket. The cooling loop also supplied water to cool the condensate. After exiting

the top of the cooling jacket the water was cooled by a shell and tube heat exchanger. The system was a closed loop in order to conserve water.

Sixteen copper-constantan (T-type) thermocouples were used to collect temperature measurements in the experiment. Ten were brazed to the outside condensing tube wall and were spaced in a logarithmic manner along the length of the tube. The remaining six thermocouples were stainless steel sheathed and were placed after the flanges inside the cooling water annulus. The spacing was also logarithmic with the closer spacing at the top of the test section. All the thermocouples wires entered the test section through the nearest flanged section. The data reduction methods used by Ogg were similar to those used by Vierow and are explained in Section 2.1.1. Ogg also had a movable wet bulb probe, but the measurements were not used in the data reduction.

2.3.2 Discussion of Results

The full test matrix is shown in Table 2.3-1. Ogg reports that the system operation was very well behaved for all flow conditions. No oscillatory behavior was observed. Ogg states that the most notable phenomenon present in the experiment was the condenser tube wall temperature inversion at the test section inlet. A typical profile is shown in Figure 2.3-2. The temperature inversion in Vierow [1990] was only present for cases of low air mass fractions. In Ogg, the inversion occurred in virtually all of the cases and it was of a different shape than that of Vierow. The Ogg data show an initial decrease in tube wall temperature followed by a peak then a decline. Vierow's inversion had an initial increase followed by a decrease. Ogg, like Siddique also found that the degradation in heat transfer on a molar basis with helium was less than the degradation caused by air. A comparison of the Ogg data with Vierow data will be made by comparing the correlations in Section 3.3.

2.3.3 Experimental Uncertainties and Analysis

The Ogg results were never published or presented in any journal or conference because of some inconsistencies in the results. Some of the runs, particularly the pure steam runs, lacked reproducibility. Thus, the f_1 correlation of Ogg is not viewed with a high degree of confidence. In addition, upon teardown of the Ogg test section it was noticed that a thermocouple on the condenser tube wall had come loose. The results are relevant, but should be viewed with some skepticism. Lessons were learned from this experiment provided the basis for improvements which were applied to the final tests done at UC Berkeley by Kuhn et al. [1993].

2.4 Kuhn (UCB)

Kuhn under the direction of Professor Schrock and Professor Peterson sought to construct an experiment which incorporated all the lessons learned from Vierow, Siddique, and Ogg. Detailed documentation will be found in Kuhn et al. [1993].

2.4.1 Apparatus

The steam supply system and the data acquisition instrumentation were nearly identical to that of Ogg. An additional steam trap was put on the steam supply line in order to insure that all the moisture was removed. The majority of the differences were found in the test section. The general schematic is shown in Figure 2.4-1.

In the Ogg experiment the condenser tube wall bare thermocouple junctions were brazed to the outer wall. In Kuhn's experiment, thermocouples were inserted into a groove machined into the condenser tube wall and the groove was filled with silver solder in a manner similar to the Siddique installation. This is illustrated in Figure 2.4-2. A heat conduction calculation was made to determine the inner and outer tube wall temperatures. The thermocouples were 0.5 mm OD SS sheathed J-type. The grooves were 12.7 mm in length. This improved installation technique is expected to result in more accurate temperature measurements and eliminate the possibility of detachment of the thermocouples from the condenser wall. The locations of the test section thermocouples are shown in Figure 2.4-3. The thermocouples located at the inner wall of the cooling jacket were 1.6 mm OD SS sheathed type thermocouples embedded in a plastic jacket. The thermocouples protruded approximately 1 mm into the cooling jacket in order to measure the coolant temperature at the adiabatic cooling jacket wall.

Perhaps the main concerns that arose from the previous three experiments were the possible variations in the degree of mixing (axially and circumferentially) in the cooling jacket and the associated effort in determining the bulk cooling water temperature. Improvements were made in each of these areas in the design of the Kuhn cooling jacket. In previous experiments there was one cooling water inlet and one cooling water outlet. In this experiment there are two inlets and four outlets spaced 90^{o} apart (shown partially in Figure 2.4-3) in order to minimize circumferential nonuniformities. The cooling jacket was constructed of a longitudinally split steel jacket. A plastic cooling jacket was first used, but this was damaged due to inadvertent addition (by a student performing a separate experiment) of steam in the condenser without any cooling water flow. The

longitudinally split cooling jacket allowed the thermocouple wires to exit the jacket radially near the axial location of their measurement instead of being led out the top or through intermediate flanges. Nylon spacers were used to fix the radial location of the cooling jacket as shown in Figure 2.4-3. The spacers and a small number of thermocouple wires were the only flow obstructions present in the cooling jacket flow annulus. There were no flanges/mixers to promote mixing as in Vierow and Ogg. The coolant flow rate was kept high enough to be naturally turbulent. The coolant bulk temperature was calculated with the aid of a computational fluid dynamics model. The model included the well-tested k-ε turbulence model which performs well in simple flows such as the annular flow in the cooling jacket. The model accounted for variations in fluid properties with temperature. With the benefit of the coolant annulus flow model, the following iterative process was developed to determine the local heat flux:

A. Fit adiabatic wall temperature to obtain an approximate heat flux:

$$q''(x) \approx -\frac{W_c c_p}{\pi D_i}\frac{dT_a(x)}{dx} \qquad 2.4\text{-}1$$

B. Inner tube wall temperature

$$T_{Win} = T_W + \frac{r_i q''(x)\ln\left(\frac{D_w}{D_i}\right)}{k_w} \qquad 2.4\text{-}2$$

C. Outer tube wall temperature

$$T_{WO} = T_{Win} + \frac{r_i q''(x)\ln\left(\frac{D_o}{D_i}\right)}{k_w} \qquad 2.4\text{-}3$$

D. Cooling water bulk temperature

$$T_{Cw} = T_{WO} - f(T_{WO}, T_a, W_c)(T_{WO} - T_a) \qquad 2.4\text{-}4$$

where $f(T_{WO}, T_a, W_c)$ is calculated by the coolant annulus numerical routine.

E. Fit cooling water temperature to obtain the improved value of heat flux:

$$q''(x) = -\frac{W_c c_p}{\pi D_i}\frac{dT_{cw}(x)}{dx} \qquad 2.4\text{-}5$$

F. Repeat steps B through E to convergence

Further details on the numerical procedure are as follows:

Velocity distribution in the annulus

$$-\frac{dP}{dz} + \frac{1}{r}\frac{\partial}{\partial r}(r\mu_{eff}\frac{\partial V_z}{\partial r}) + \rho g = 0 \qquad 2.4\text{-}6$$

By solving this momentum equation, the fully developed velocity profile V_Z is obtained when μ_{eff} is derived by solving the turbulent k-ε equation in which temperature dependence of properties was taken into account.

Temperature distribution in the annulus

$$\rho C_p(v_z\frac{\partial T}{\partial z} + v_r\frac{\partial T}{\partial r}) = \frac{1}{r}\frac{\partial}{\partial r}(rk_{eff}\frac{\partial T}{\partial r}) \qquad 2.4\text{-}7$$

or

$$\rho C_p v_z\frac{dT_b}{dz} = \frac{1}{r}\frac{\partial}{\partial r}(rK_{eff}\frac{\partial T}{\partial r}) \text{ for } v_r = 0 \text{ and } \frac{dT_b}{dz} = \frac{\partial T}{\partial z} \qquad 2.4\text{-}8$$

with boundary conditions

$T_b = T_{bw}$ at $z = 0$

$T = T_i$ at $r = R_i$

$T = T_o$ at $r = R_o$

$k_{eff} = k(r)$ for laminar flow (Thermal conductivity k(T))

$k_{eff} = k(r) + k_t(r)$ for turbulent flow

$= k(r) + c_p\mu_t$

Bulk Temperature

The cooling water bulk temperature by definition is given as

$$T_{Cw} = \frac{\int_{R_i}^{R_o} T(r) v_z(r) dr}{\int_{R_i}^{R_o} v_z(r) dr} \qquad 2.4\text{-}9$$

and the cooling water bulk temperature ratio f is defined as

$$f = \frac{T_i - T_b}{T_i - T_o} = \frac{T_{wo} - T_b}{T_{wo} - T_a} \qquad 2.4\text{-}10$$

and this is used in equation 2.4-4 to obtain T_b from measured values of the outside tube wall temperature and the cooling jacket adiabatic temperature T_a.

2.4.2 Results

The complete results will be available in Kuhn et al. [1993]. At the time of this report only limited results were available in a plotted form. These results will be discussed in Section 3.6. A test matrix is shown in Table 2.4-1..

THIS PAGE IS INTENTIONALLY BLANK.

Run No.	Inlet Air Mass Frac.	Inlet Temp. (°C)	Inlet steam flowrate (kg/hr)
1	0.09	100.0	8.93
2	0.15	100.0	8.83
3	0.18	100.2	8.76
4	0.24	100.0	9.15
5	0.29	100.1	9.12
6	0.33	100.0	9.09
7	0.08	119.9	9.39
8	0.14	119.9	9.30
9	0.19	119.9	9.24
10	0.26	119.6	8.97
11	0.33	120.0	9.38
12	0.42	119.9	8.80
13	0.11	140.0	7.98
14	0.18	139.9	8.04
15	0.24	139.9	7.95
16	0.30	139.9	8.00
17	0.34	139.9	7.92
18	0.12	100.0	20.02
19	0.17	100.1	19.85
20	0.21	100.2	19.82
21	0.25	100.2	19.99
22	0.31	100.0	19.68
23	0.35	100.0	19.82
24	0.11	120.0	20.42
25	0.15	120.0	20.84
26	0.22	119.9	20.67

Run No.	Inlet Air Mass Frac.	Inlet Temp. (°C)	Inlet steam flowrate (kg/hr)
27	0.27	119.9	20.70
28	0.31	119.9	20.35
29	0.36	119.9	20.65
30	0.10	140.0	19.95
31	0.15	140.2	19.73
32	0.20	140.2	19.92
33	0.25	140.0	20.37
34	0.32	140.0	19.90
35	0.11	100.0	25.34
36	0.14	100.5	27.08
37	0.19	100.5	28.63
38	0.24	100.5	28.84
39	0.30	100.5	28.76
40	0.35	100.5	28.97
41	0.10	120.1	30.41
42	0.15	120.1	30.97
43	0.20	120.1	30.35
44	0.24	120.1	29.91
45	0.31	120.1	29.41
46	0.34	120.1	29.61
47	0.10	140.0	31.91
48	0.15	140.0	31.75
49	0.20	140.0	31.90
50	0.25	140.1	31.61
51	0.30	140.1	31.41
52	0.35	140.1	31.09

Table 2.2-1a: Test matrix for air/steam runs of Siddique

Run No.	Inlet He Mass Frac.	Inlet Temp. (°C)	Inlet steam flowrate (kg/hr)
1	0.02	101.2	8.93
2	0.04	101.2	8.83
3	0.07	101.3	8.76
4	0.10	100.8	9.15
5	0.02	120.0	9.12
6	0.05	120.0	9.09
7	0.08	120.1	9.39
8	0.11	119.7	9.30
9	0.03	139.2	9.24
10	0.04	139.6	8.97
11	0.06	139.3	9.38
12	0.02	101.9	8.80
13	0.04	102.9	7.98
14	0.05	103.5	8.04
15	0.07	103.9	7.95
16	0.02	119.4	8.00
17	0.05	120.4	7.92
18	0.07	120.3	20.02
19	0.09	120.3	19.85
20	0.02	141	19.82
21	0.04	140.9	19.99
22	0.05	140.8	19.68

Table 2.2-1b: Test matrix for helium/steam runs of Siddique

TEST RUN NUMBERS

(Numbers identify test runs performed in chronological order)

	Steam flow in kg/hr (lbm/hr)					
	72.7 (160.0)	61.4 (135.0)	50.0 (110.0)	38.6 (85.0)	27.3 (60.0)	15.9 (35.0)
Air flow (%)						
40.0	**	**	14.1	13.1	14.2	11.3
15.0	13.4	13.3	13.2	12.4	11.4	16.2
10.0	12.1	12.2	12.3	15.4	16.1	18.3
5.0	15.1	15.2	15.3	17.4	18.1	18.4
2.0	17.1	17.2	17.3	19.4	18.2	**
1.0	19.1	19.3	19.2	**	**	**
0.5	**	**	**	**	**	**
0.0	8.1	8.2	8.3	10.3	11.1	11.2
He (%)						
5.0	**	**	**	**	21.1	21.3
2.0	25.1	25.2	25.3	20.4	21.2	21.4
1.0	20.1	20.2	20.3	23.4	24.1	24.2
0.5	23.1	23.2	23.3	24.3	**	**

Table 3.2-1a: Test matrix for Ogg experiment. Used with permission.

SYSTEM INLET PRESSURES (ABSOLUTE)

RUN #	Inlet P. (kPa)		RUN #	Inlet P. (kPa)
8.1	115.09		19.1	186.14
8.2	103.64		19.2	153.94
8.3	98.34		19.3	179.93
10.3	97.92		19.4	139.12
11.1	100.05		20.1	273.90
11.2	98.88		20.2	215.78
11.3	105.64		20.3	126.97
11.4	105.64		20.4	160.41
12.1	110.47		21.1	144.81
12.2	110.67		21.2	108.95
12.3	109.91		21.3	109.78
12.4	107.78		21.4	104.06
13.1	121.98		23.1	189.33
13.2	119.15		23.2	134.79
13.3	131.84		23.3	156.03
13.4	143.70		23.4	137.28
14.1	122.07		24.1	106.88
14.2	106.56		24.2	104.95
15.1	285.50		24.3	132.46
15.2	142.98		25.1	306.61
15.3	123.75		25.2	192.43
15.4	138.98		25.3	176.44
16.1	152.69		27.1	101.38
16.2	123.46		27.2	100.07
17.1	251.73		27.3	92.63
17.2	145.14		27.4	95.32
17.3	132.59		27.5	112.76
17.4	125.56		27.6	100.83
18.1	117.59			
18.2	104.90			
18.3	110.42			
18.4	105.66			

Table 3.2-1b: Test matrix for Ogg experiment. Used with permission.

Experimental Test Matrix

P : Test section inlet pressure (atm)

Ws : Steam inlet flow rate (kg/hr)

Ma : Air inlet mass fraction

Mh : Helium inlet mass fraction

Series PS-I (Pure steam) : 42 runs

Ws P	1 atm	2 atm	3 atm	4 atm	5 atm
60	1.1-1	1.1-2	1.1-3	1.1-4	1.1-5
50	1.2-1	1.2-2	1.2-3	1.2-4	1.2-5
40	1.3-1	1.3-2	1.3-3	1.3-4	1.3-5
30	1.4-1	1.4-2	1.4-3	1.4-4	1.4-5
60 (R)	1.1-1R	1.1-2R	1.1-3R	1.1-4R1	1.1-5R1
40 (R)	1.3-1R1	1.3-2R1	1.3-3R1	1.3-4R1	1.3-5R1
Extra:	1.1-4R2	1.1-4R3	1.1-5R2	1.1-5R3	1.2-4R1
	1.2-5R1	1.3-1R2	1.3-2R2	1.3-3R2	1.3-4R2
	1.3-5R2	1.4-4R1			

Series NC-I (air-steam mixture) : 32 runs

Ws = 50 kg/hr, P = 4atm					
Ma		Ma		Ma	
1%	2.1-1	8%	2.1-6	25%	2.1-10
2%	2.1-2	10%	2.1-7	30%	2.1-11
3%	2.1-3	15%	2.1-8	35%	2.1-12
4%	2.1-4	20%	2.1-9	40%	2.1-13
6%	2.1-5				
3% (R)	2.1-3R	8% (R)	2.1-6R	25% (R)	2.1-10R
6% (R)	2.1-5R	15% (R)	2.1-8R	35% (R)	2.1-12R
Extra :13 runs at same air mass fraction but 1 atm :					2.2-1
2.2-2	2.2-3	2.2-4	2.2-5	2.2-6	2.2-7
2.2-8	2.2-9	2.2-10	2.2-11	2.2-12	2.2-13

Table 3.3-1a: Test matrix for Kuhn [1993] experiment. R = repeat runs

Experimental Test Matrix (continued)

P : Test section inlet pressure (atm)
Ws : Steam inlet flow rate (kg/hr)
Ma : Air inlet mass fraction
Mh : Helium inlet mass fraction

Series NC-II (air-steam mixture) : 39 runs

	Ws = 60 kg/hr			Ws = 30 kg/hr		
Ma P	2 atm	3 atm	5 atm	2 atm	3 atm	5 atm
1%	3.1-2	3.1-3	3.1-5	4.1-2	4.1-3	
5%	3.2-2	3.2-3	3.2-5	4.2-2	4.2-3	4.2-5
10%	3.3-2	3.3-3	3.3-5	4.3-2	4.3-3	4.3-5
20%	3.4-2	3.4-3	3.4-5	4.4-2	4.4-3	4.4-5
40%	3.5-2	3.5-3	3.5-5	4.5-2	4.5-3	4.5-5
Extra	3.1-4	3.2-1	3.2-4	3.3-1	3.3-4	3.4-2R1
	3.2-3R1	3.5-2R1	3.5-3R1	3.5-4		

Series NC-III (He-steam mixture) : 24 runs

	P = 4 atm			
Mh Ws	30	45	60	45(R)
0.30%	5.1-1	5.2-1	5.3-1	5.2-1R
0.50%	5.1-2	5.2-2	5.3-2	5.2-2R1
1%	5.1-3	5.2-3	5.3-3	5.2-2R2
3%	5.1-4	5.2-4	5.3-4	5.2-4R
5%	5.1-5	5.2-5	5.3-5	5.2-5R
10%	5.1-6	5.2-6		5.2-6R
15%	5.1-7			

Table 3.3-1b: Test matrix for Kuhn [1993] experiment.

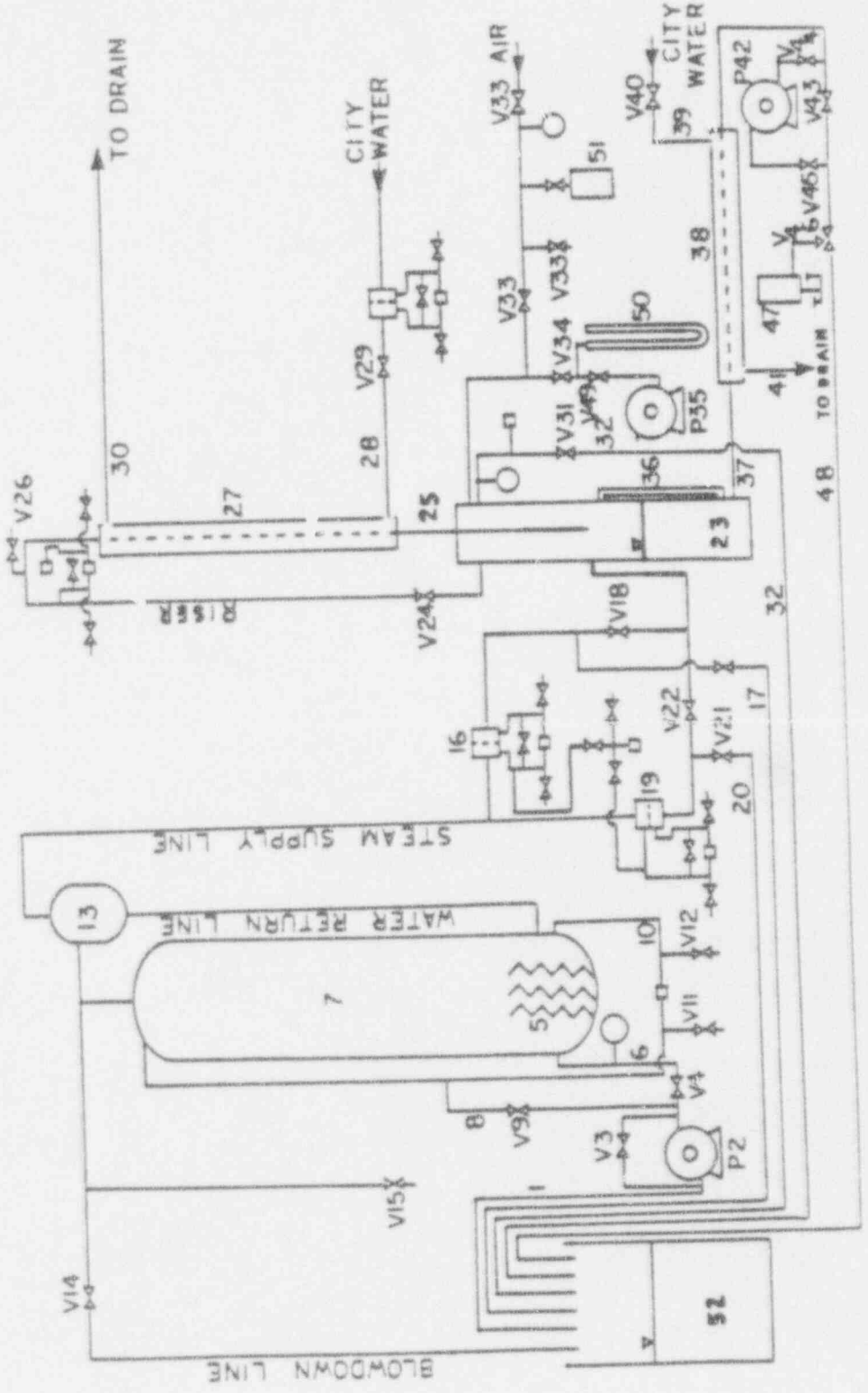

Figure 2.1-1a Schematic of Vierow [1990] experiment Used with permission

KEY TO SYSTEM SCHEMATIC

Component	Description
1	Water feed line from reservoir
P2	Reservoir fill pump
V3	Pump bypass valve
V4	Regulating valve for reservoir fill line
5	Immersion heaters
6	Reservoir fill line
7	Steam/water pressure reservoir
8	Fill line to purge pressure sense line of air
V9	Regulating valve for filling pressure sense line
10	Reservoir level sense lines
V11	Valve to purge pressure sense line of air
V12	Valve to purge pressure sense line of air
13	Steam/air separator
V14	Pressure relief valve
V15	Air intake valve
16	Orifice meter on 1/2-inch steam supply line
17	Steam/air purge line on 1/2-inch steam line
V18	Valve on 1/2-inch steam supply line
19	Orifice meter on 1-inch steam supply line
20	Steam/air purge line on 1-inch steam supply line
V21	Regulating valve on steam/air purge line
V22	Valve on 1-inch steam supply line
23	Lower chamber
V24	Gate valve
25	Downcomer
V26	High-point vent valve
27	Condensation test section
28	Test section coolant inlet line
V29	Regulating valve for test section coolant
30	Test section coolant outlet line
V31	Pressure relief valve
32	Test loop blowdown line to barrel
V33	Air intake valves
V34	Manometer to loop isolation valve
P35	Vacuum pump
36	Sight glass
37	Condensate drain line
38	Condensate heat exchanger
39	Condensate coolant inlet line
V40	Regulating valve for condensate coolant inlet
41	Condensate coolant outlet line
P42	Condensate pump
V43	Pump bypass valve
V44	Regulating valve for condensate pump
V45	Regulating valve for condensate pump
V46	Three-way valve to direct condensate flow
47	Condensate measurement tank and weighing scale
48	Return line to supply barrel
V49	Manometer to vacuum pump isolation valve
50	Mercury manometer
51	Pressurized air bottle
52	Water Reservoir/Quench Tank

Figure 2.1-1b Key to system schematic of Vierow [1990] experiment. Used with permission.

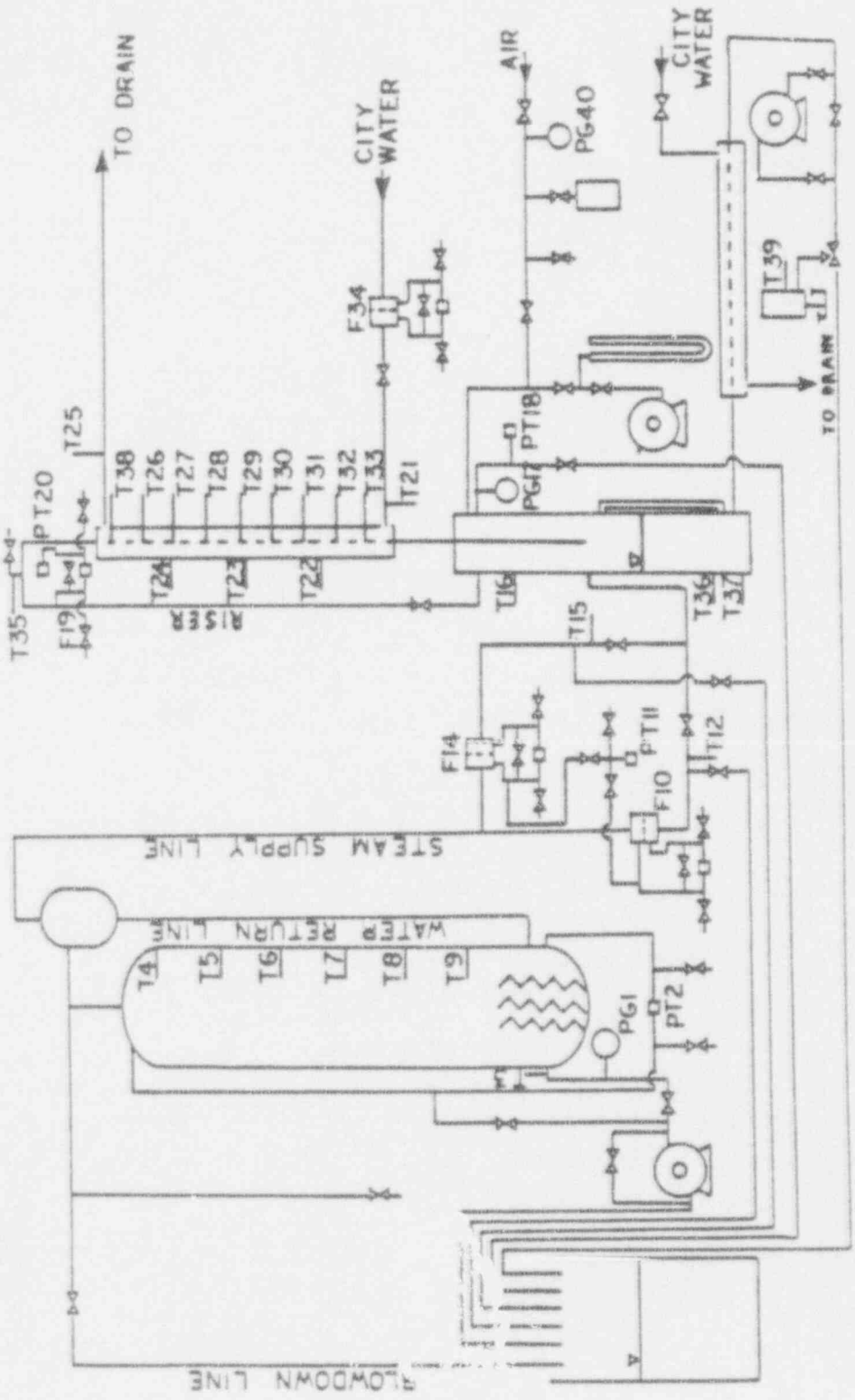

FIGURE 5 EXPERIMENTAL INSTRUMENTATION

Figure 2.1-2a Experimental instrumentation of Vierow [1990] experiment. Used with permission

KEY TO INSTRUMENTATION DIAGRAM

Component Number	Description
PG0	Visual gauge for vessel gauge pressure
PT2	Diff. PT on reservoir level sense line
T3	Pressure vessel water TC
T4 -> T9	Pressure vessel wall TC's
F10	Flow meter on 1-inch steam supply line
PT11	PT on 1-inch and 1/2-inch steam supply line
T12	1-inch steam supply inlet TC
F14	Flow meter on 1/2-inch steam supply line
T15	1/2-inch steam supply inlet TC
T16	Lower chamber TC
PG17	Visual pressure gauge on lower chamber
PT18	PT on lower chamber
F19	Flow meter on steam/air entering test section
PT20	Diff. PT for absolute pressure at top of loop
T21	Test section coolant inlet TC
T22 -> T24	Test section coolant bulk temperature TC's
T25	Test section coolant outlet TC
T26 -> T33	Condensor tube outer wall temperature TC's
F34	Flow meter on test section coolant line
T35	Test loop high point TC
T36	Condensate TC
T37	Condensate TC
T38	Condensor tube outer wall temperature TC
T39	Condensate drain TC
PG40	Gauge on pressurized air bottle

F	= flow meter
PG	= pressure gauge
PT	= pressure transducer
TC	= thermocouple
Diff.	= differential

Figure 2.1-2b: Key to experimental instrumentation of Vierow [1990] experiment. Used with permission.

TYPICAL STEADY-STATE TEST SECTION TEMPERATURE PROFILES

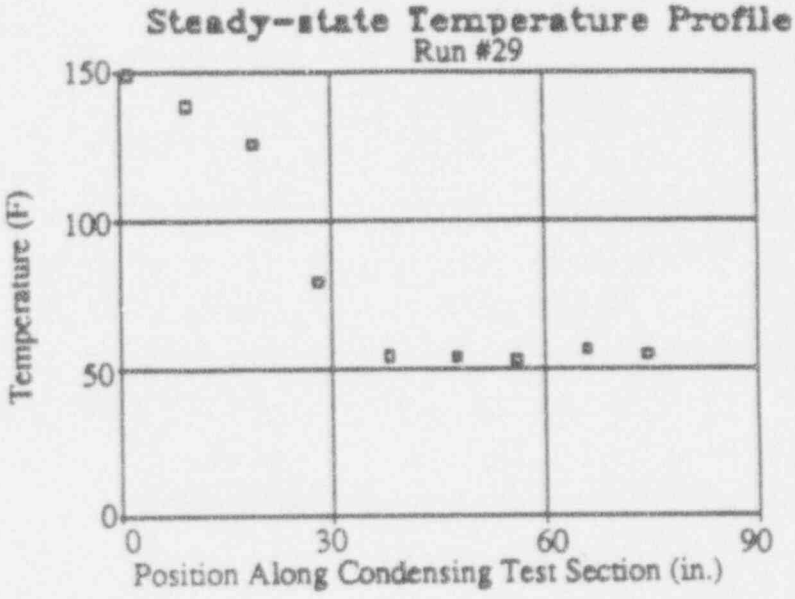

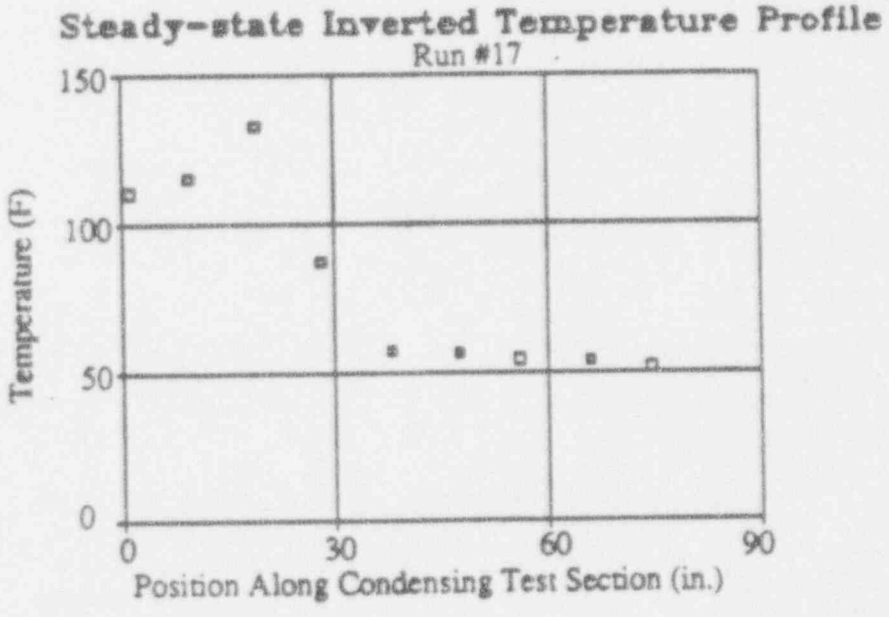

Figure 2.1-3: Typical steady-state condenser tube wall temperatures for Vierow [1990] experment. Used with permission.

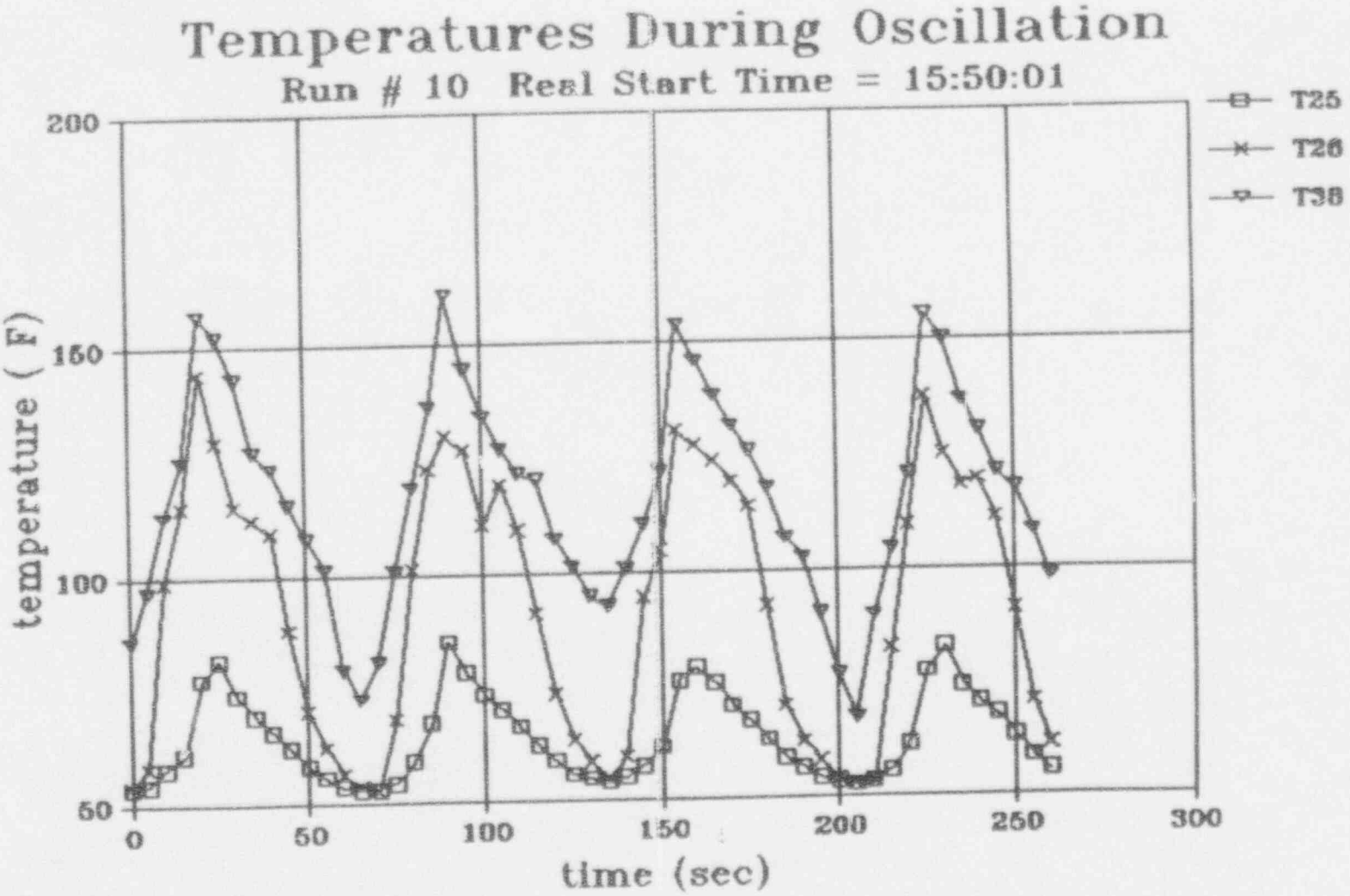

Figure 2.1-4. Sample thermocouple time records for an oscillatory run of Vierow [1990]. Used with permission.

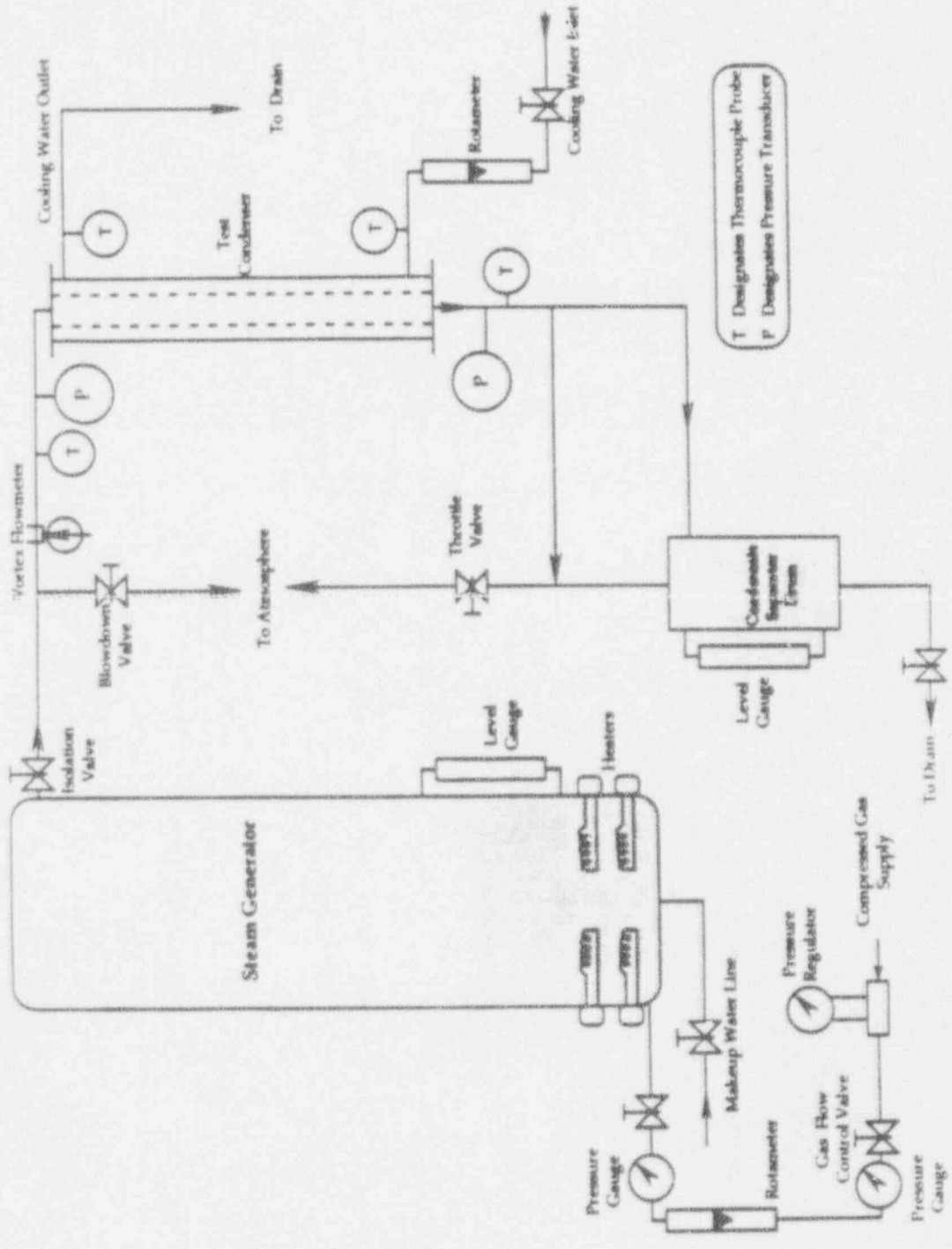

Figure 2.2-1 Schematic of Siddique [1992] experiment. Used with permission.

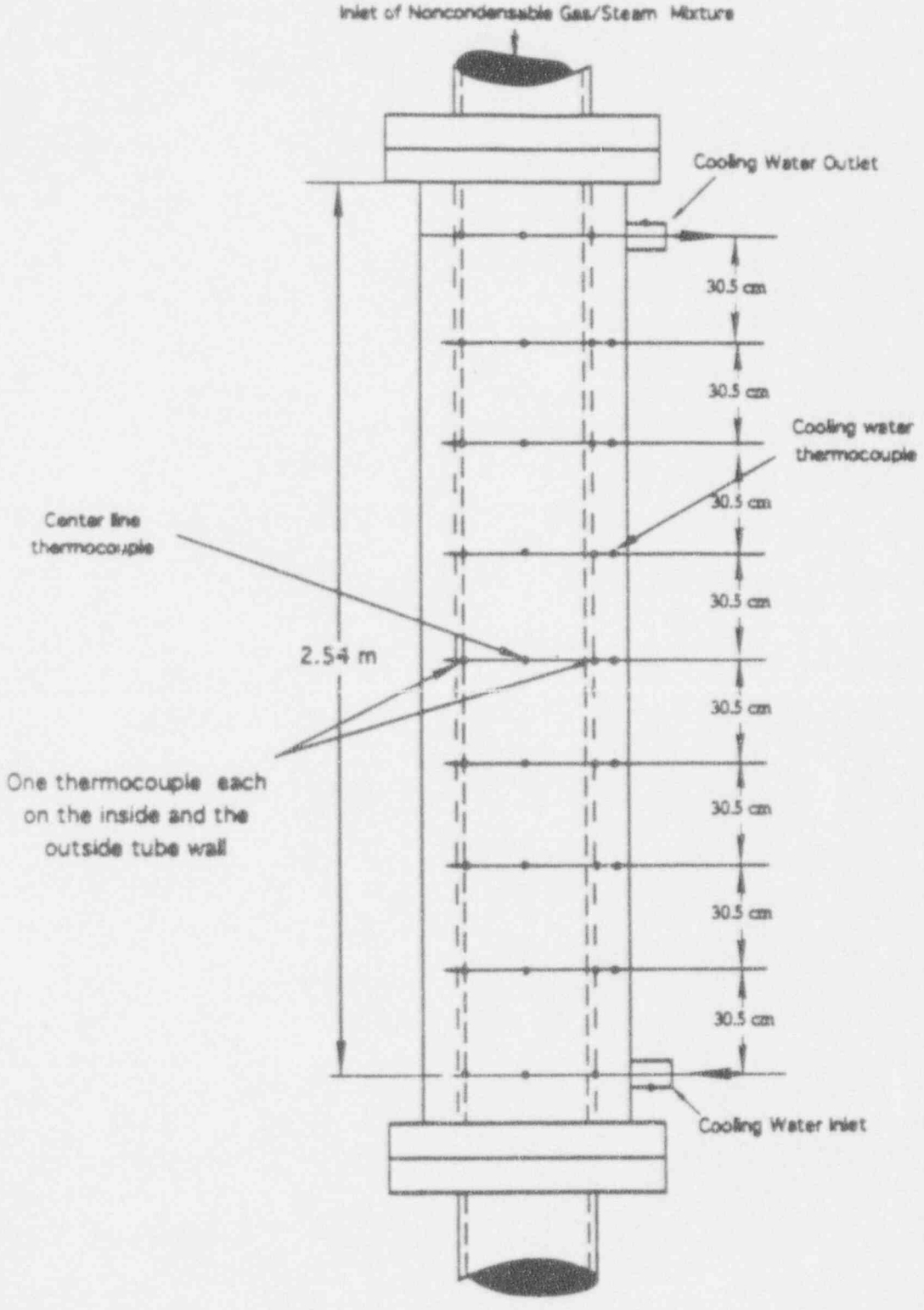

Figure 2.2-2: Test section and thermocouple configuration for Siddique [1992] experiment. Used with permission.

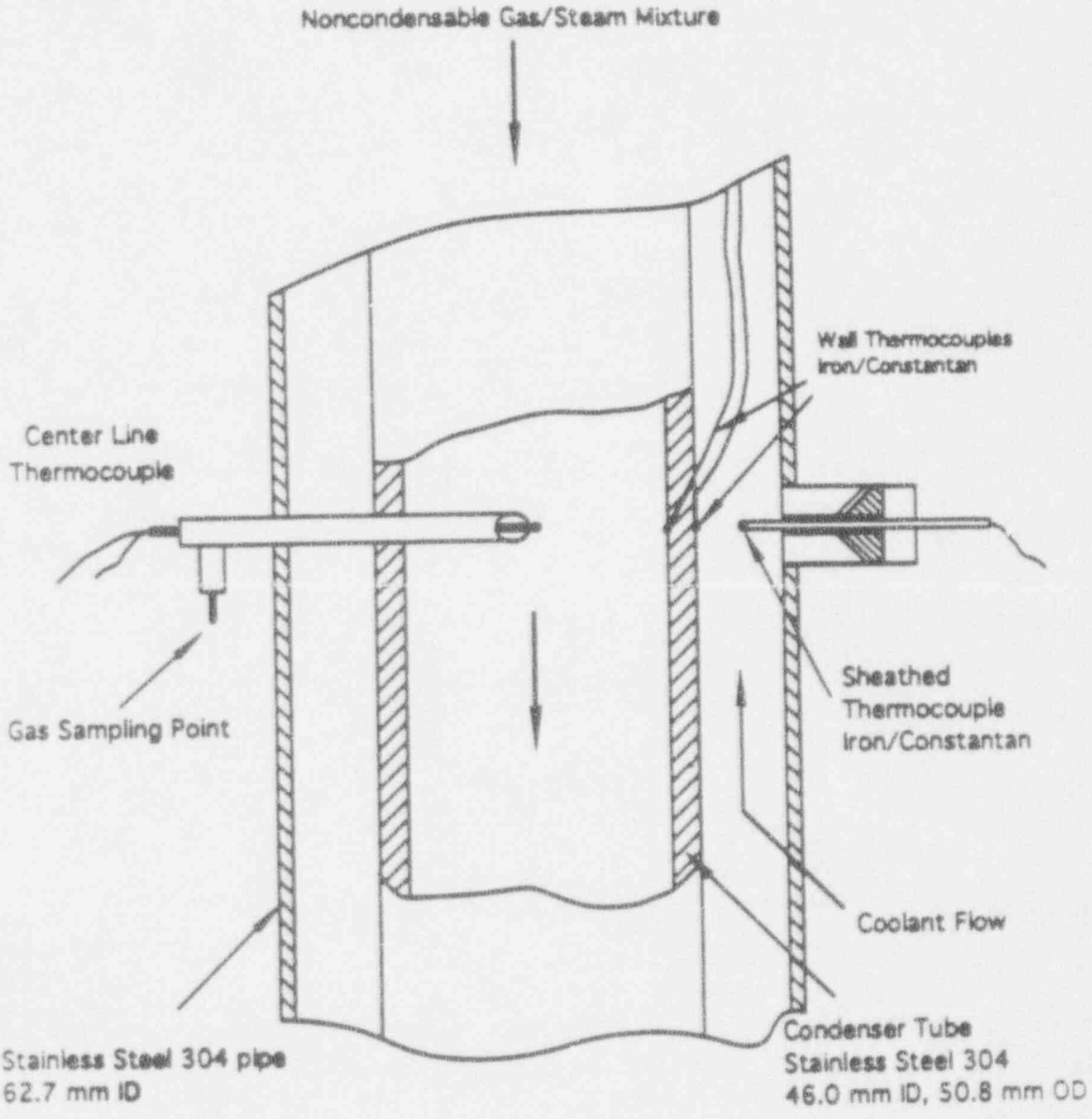

Figure 2.2-3: Detail of test section instrumentation for Siddique [1992] experiment. Used with permission.

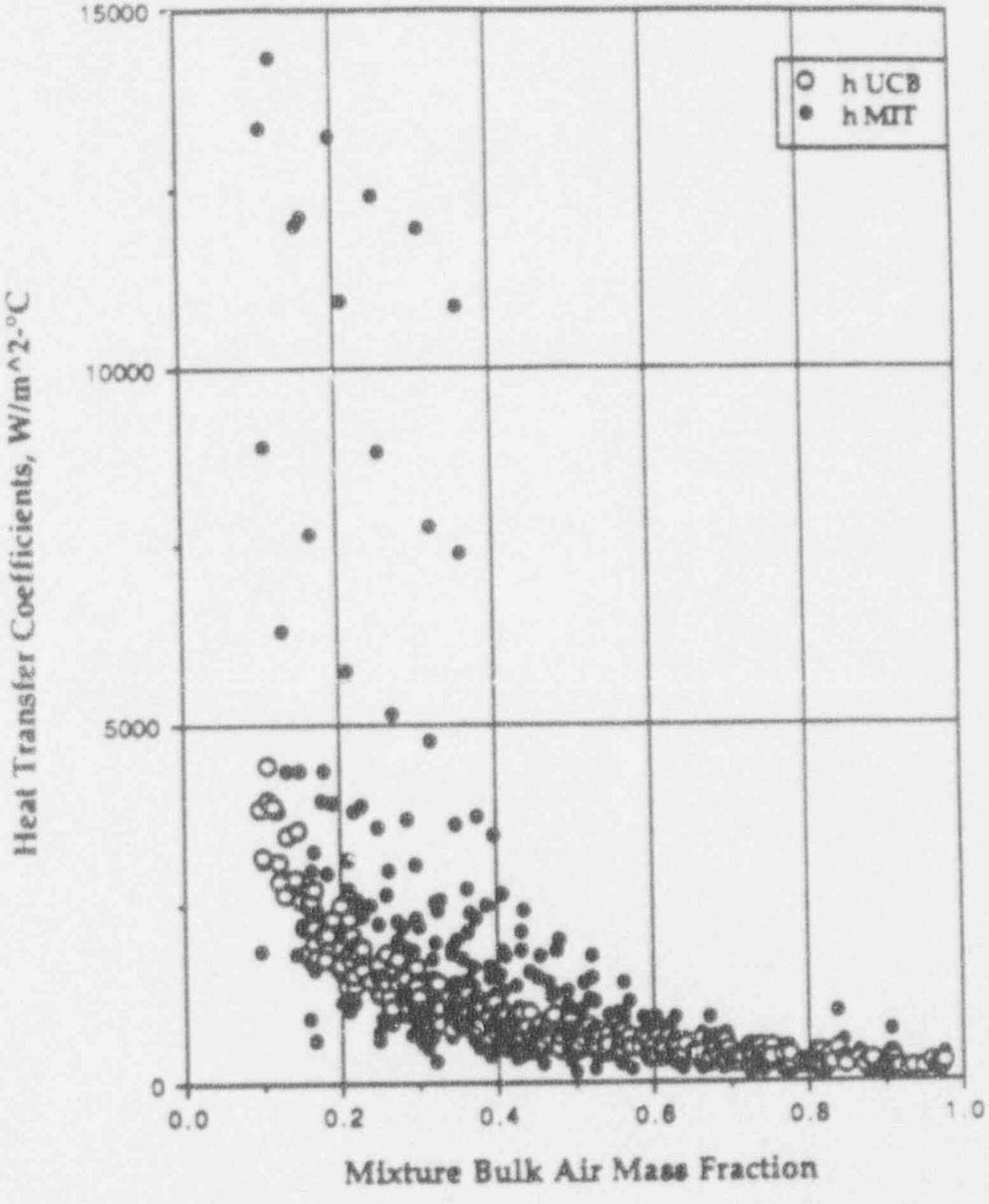

Figure 2.2-4. Plot of heat transfer coefficient as predicted by the Siddique correlation and the Vierow [1990] (not Vierow and Schrock) versus mixture bulk air mass fraction. Taken from Siddique [1992] and used with permission.

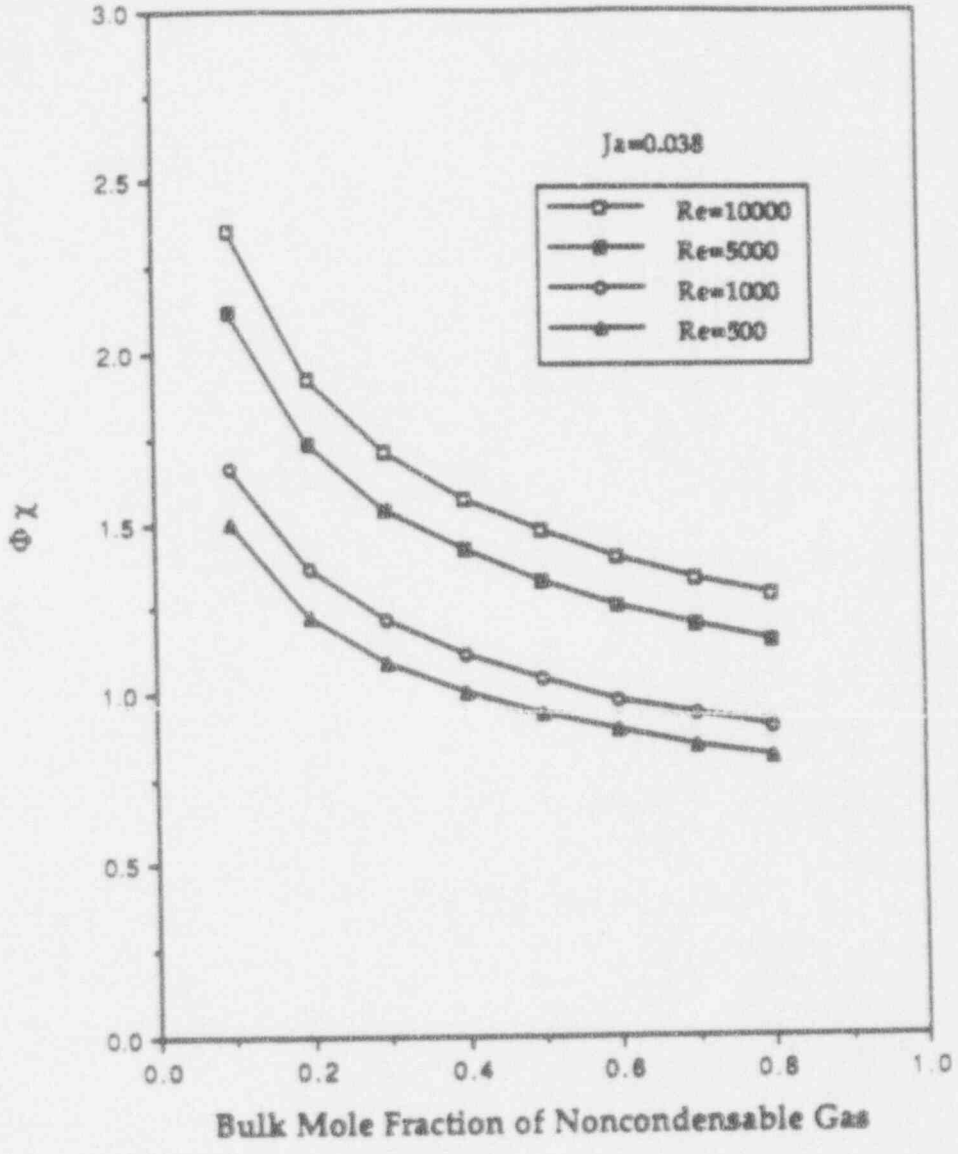

Figure 2.2-5: Ratio of Nusselt numbers when helium is present versus when air is present plotted versus the **mole** fraction of noncondensable gas. Taken from Siddique [1992] and used with permission.

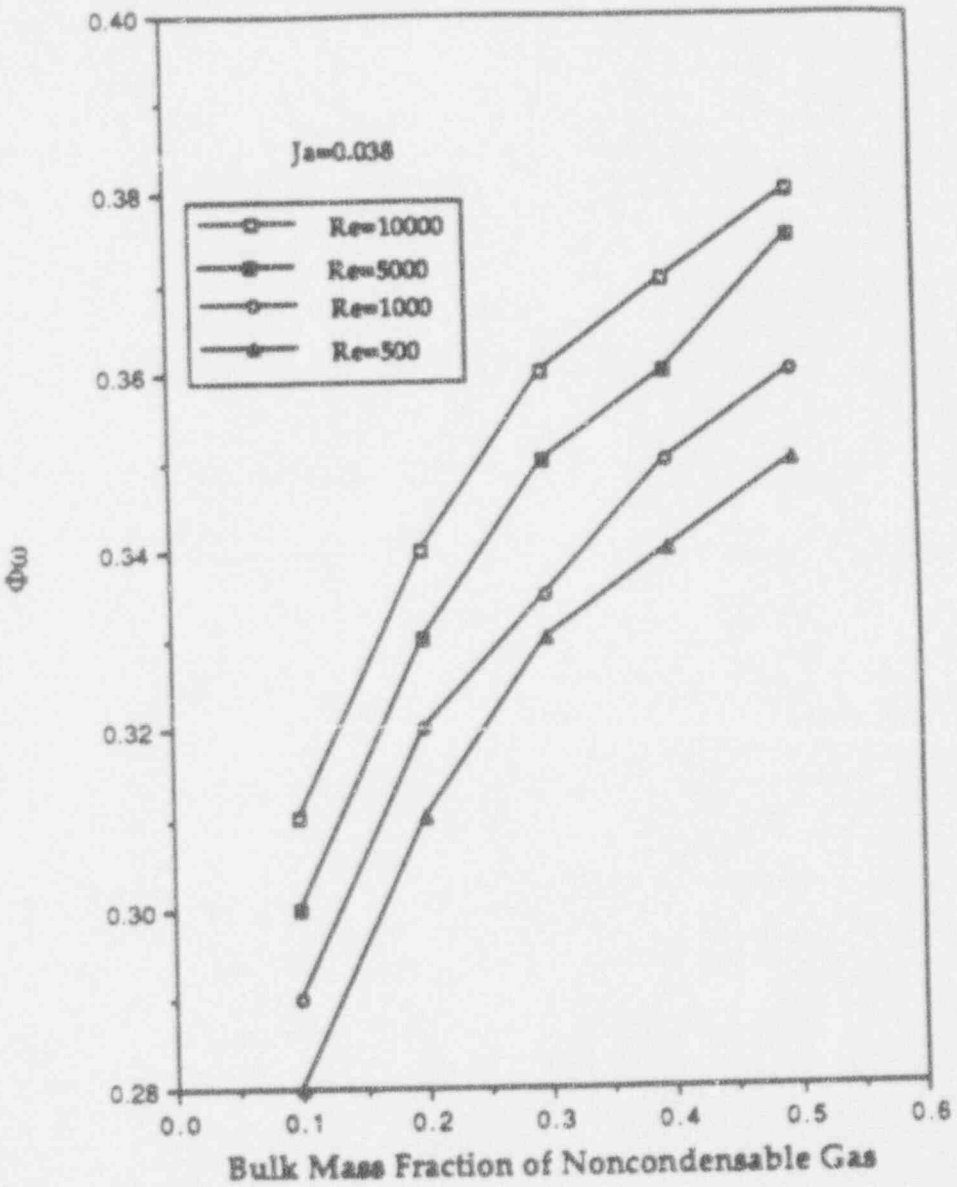

Figure 2.2-6. Ratio of Nusselt numbers when helium is present versus when air is present plotted versus the mass fraction of noncondensable gas. Taken from Siddique [1992] and used with permission.

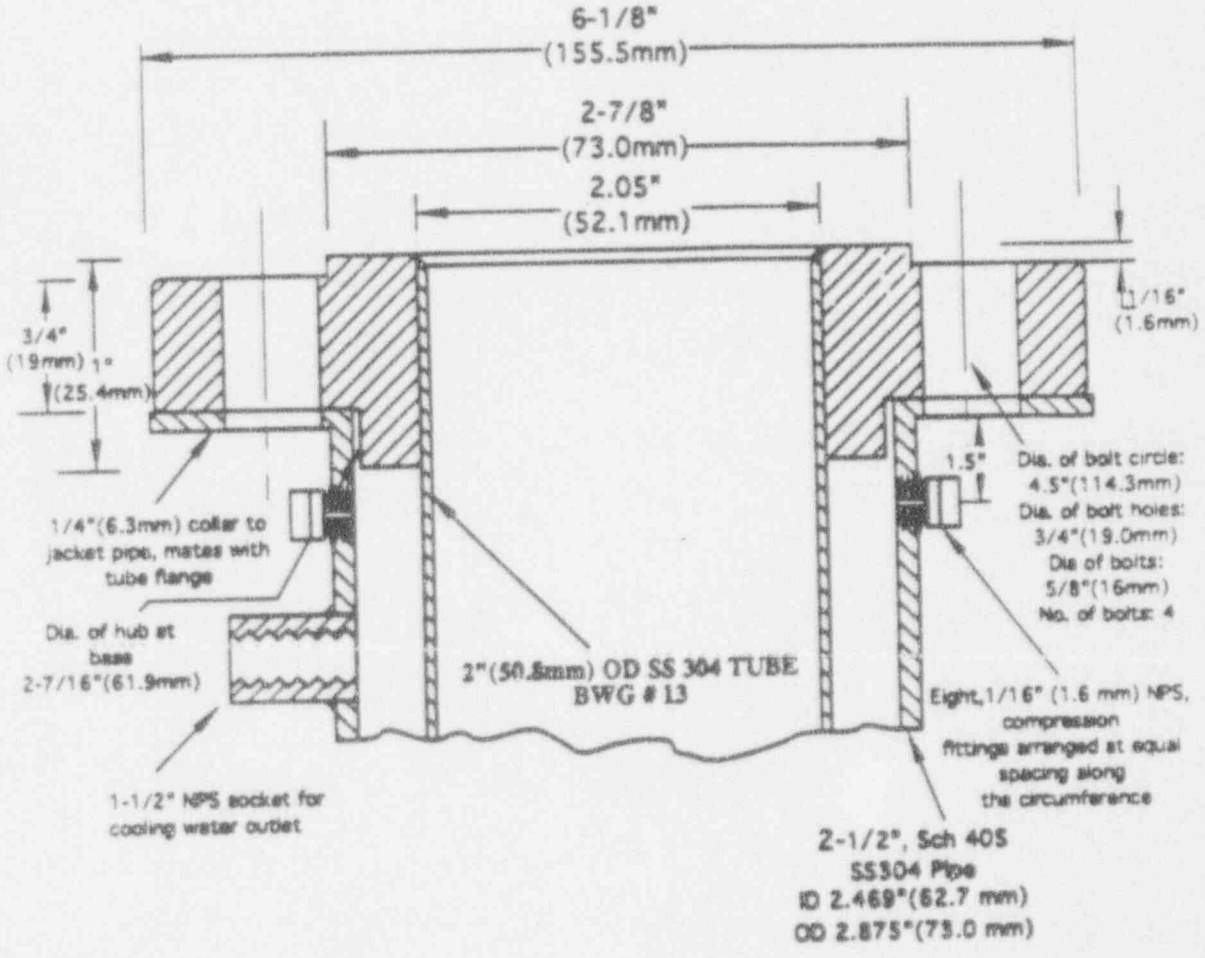

Figure 2.2-7: Detailed sketch of the upper part of Siddique's [1992] test section. Used with permission.

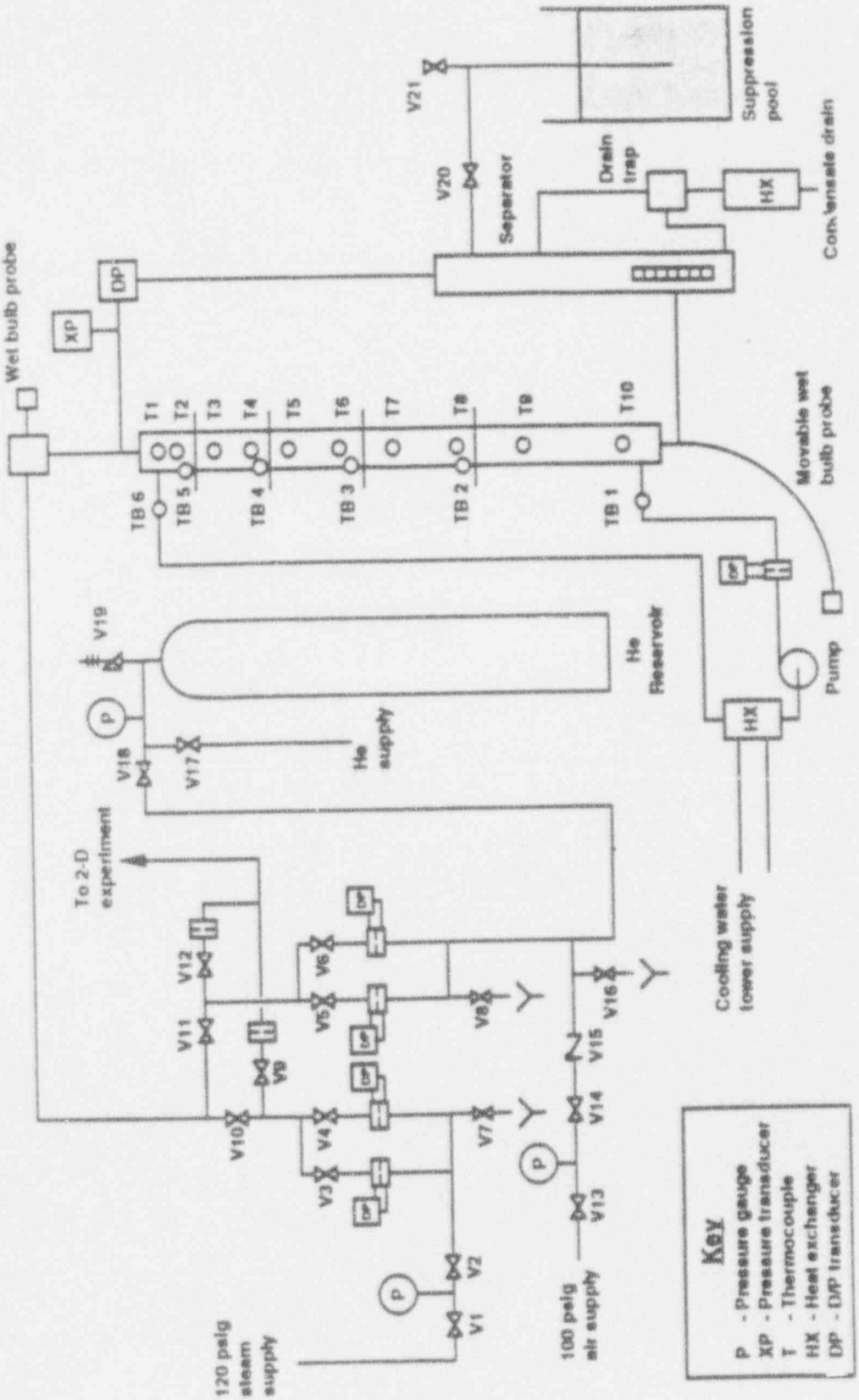

Figure 2.3-1 System schematic of Ogg [1991] experiment. Used with permission

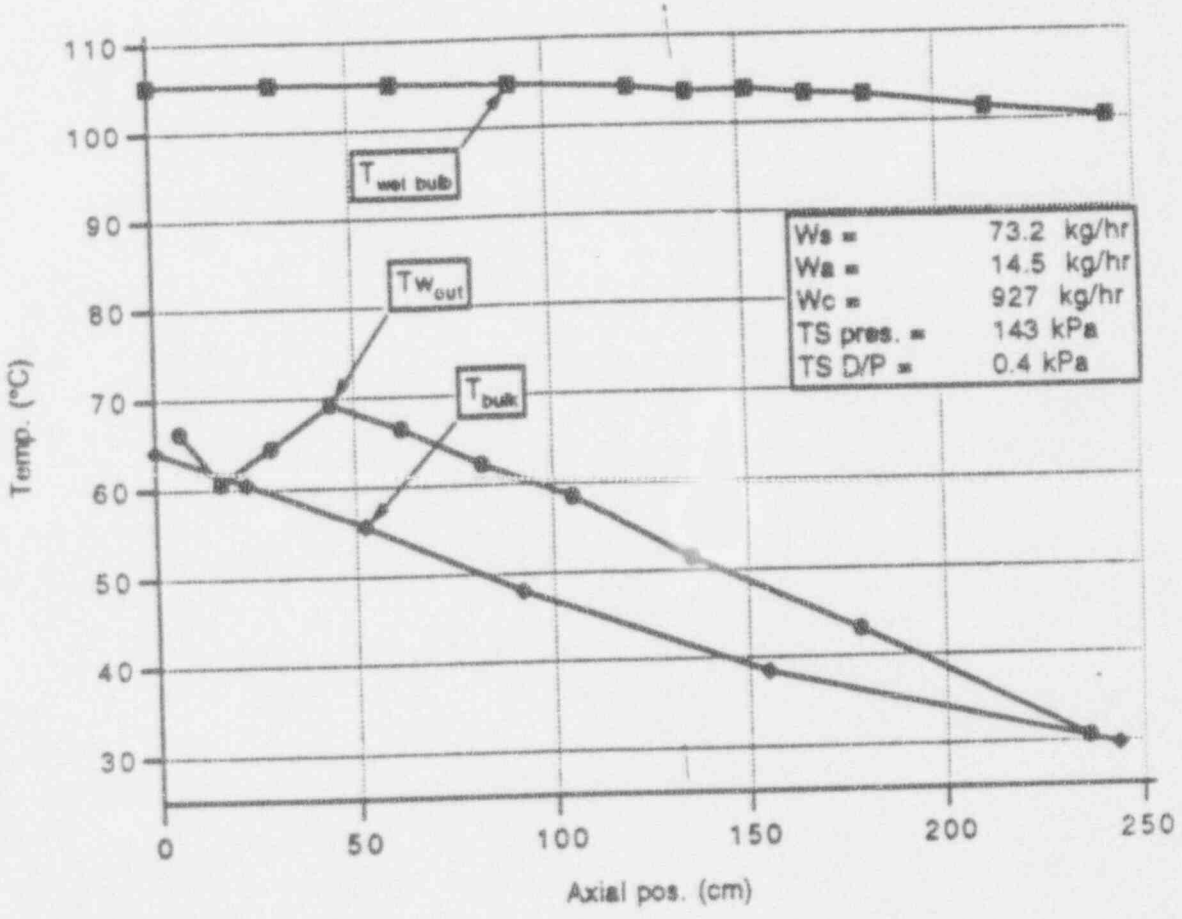

Figure 2.3-2: Typical temperature profiles from Ogg [1991]. Used with permission.

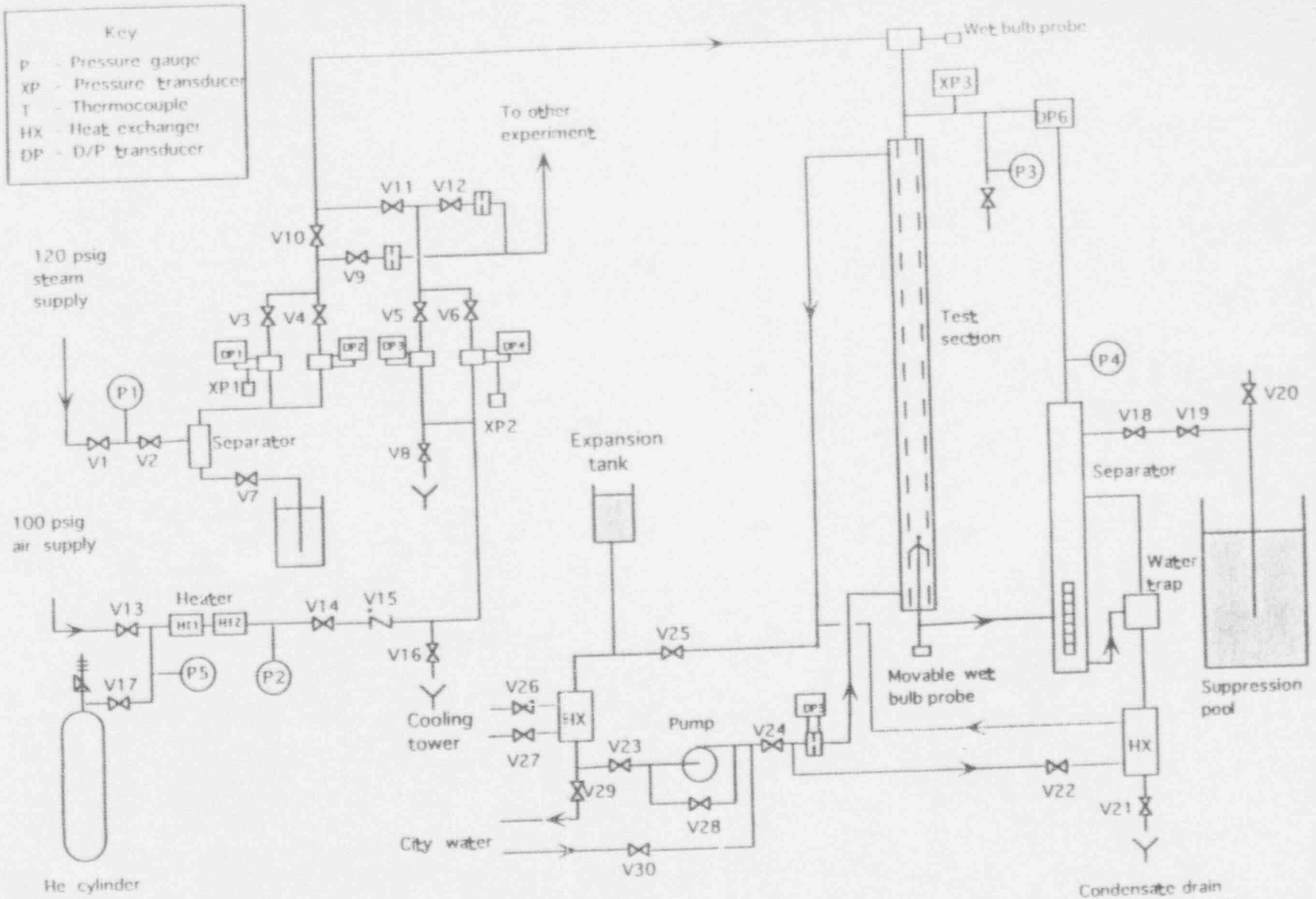

Figure 2.4-1: General schematic drawing of Kuhn et al. [1993] experimental apparatus

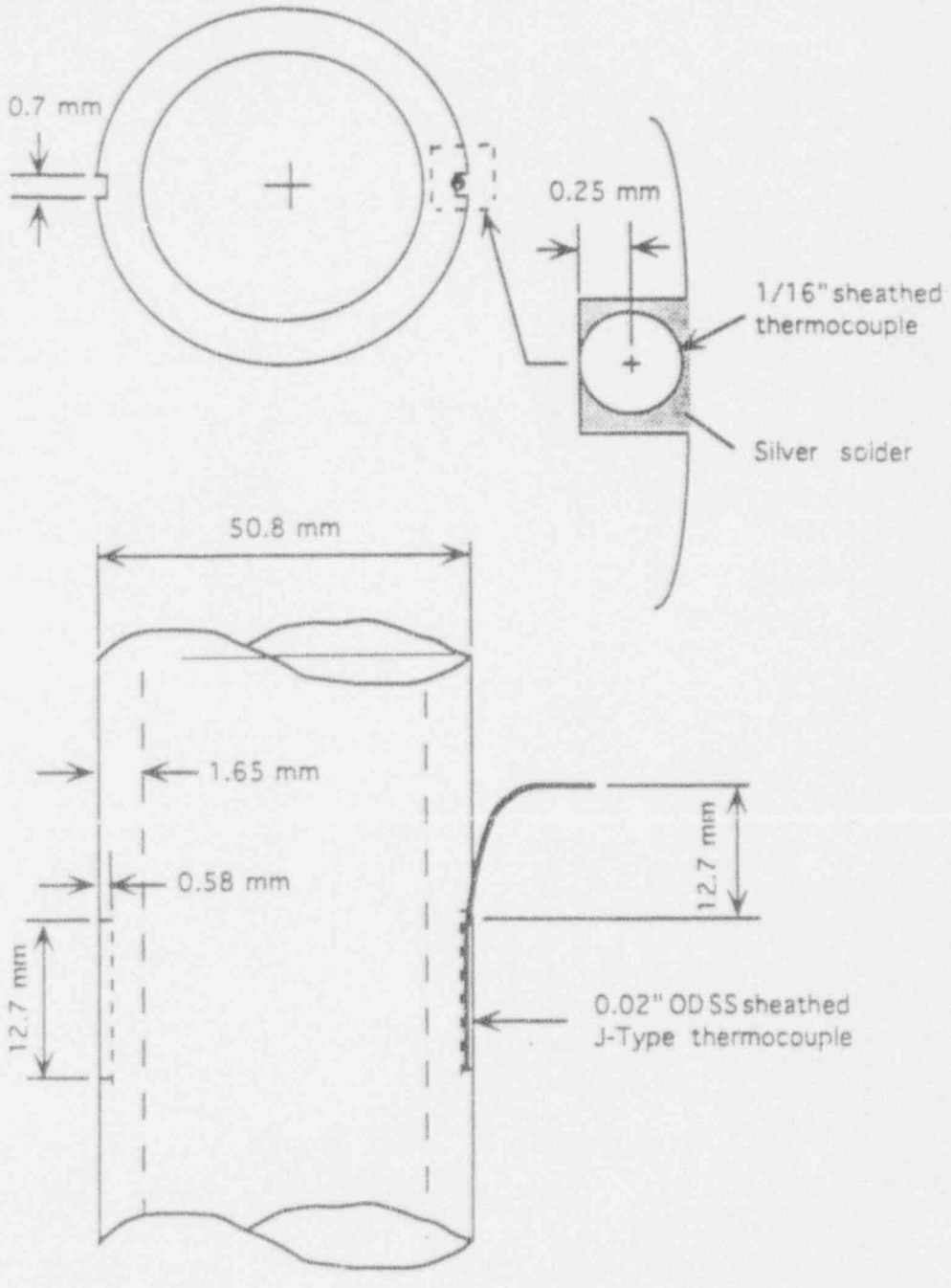

Figure 2.4-2: Sketch showing the condensing tube thermocouple installation in Kuhn et al. [1993].

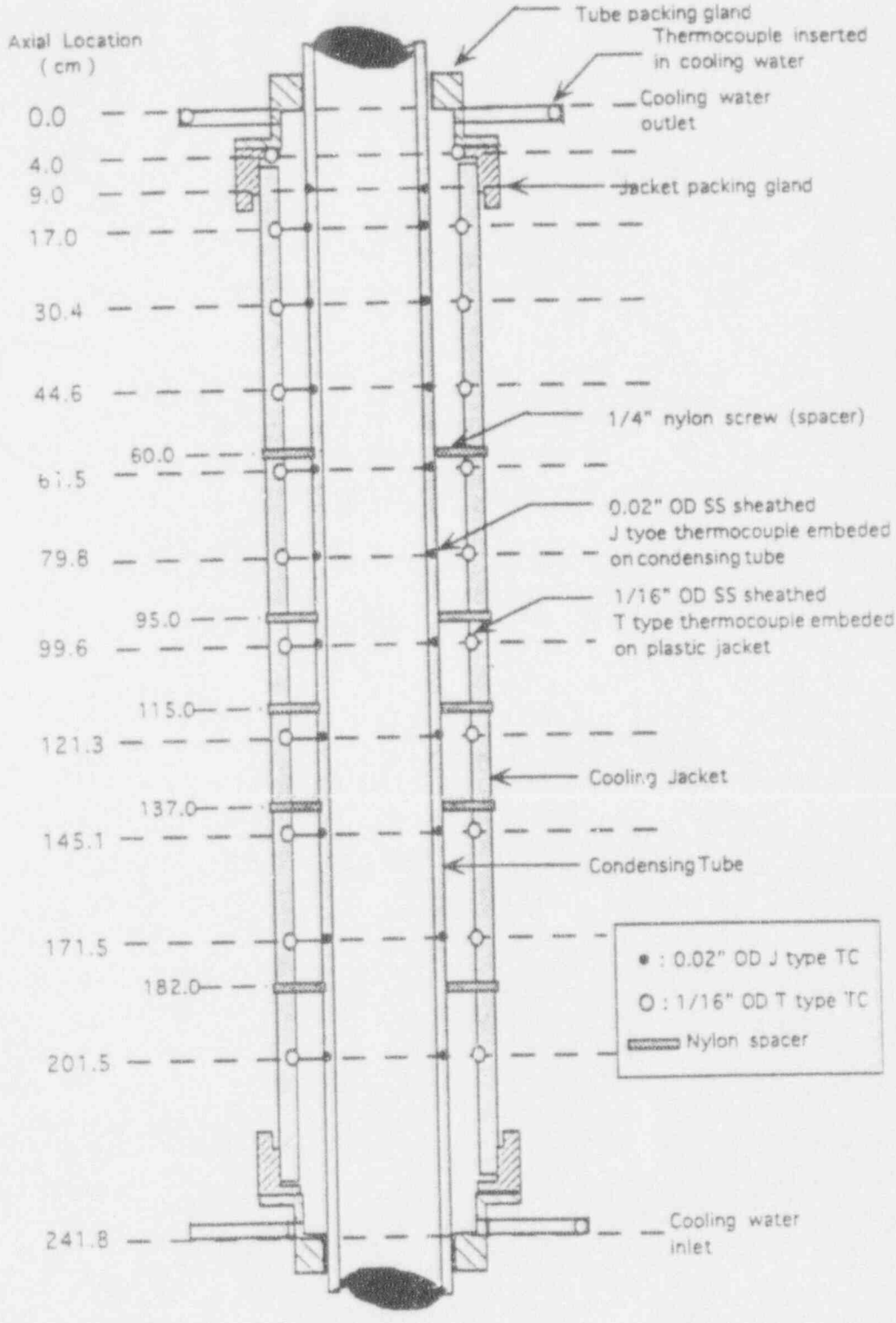

Figure 2.4-3. Test section thermocouple and spacer locations for Kuhn et al. [1993] experiment.

3. CORRELATIONS

3.1 Vierow and Schrock ("Tsukuba")

The correlation currently in TRACG is based on a slightly modified version of the correlation presented in Vierow and Schrock [1991]. The database used was the database developed by Vierow [1990]. The Tsukuba correlation, as noted in Section 2.2.2, differs from that presented in Vierow [1990]. The Tsukuba database excluded the runs which did not reach a steady-state condition as well as the runs with the temperature inversions.

The data were correlated as a two-part correction to a reference local heat transfer coefficient. This reference heat transfer coefficient is termed the "Nusselt" heat transfer coefficient. This reference value is calculated by dividing the condensate thermal conductivity by the local liquid film thickness as calculated from the model of smooth interface, gravity-driven laminar film flow:

$$\delta_1 = \left(\frac{3\mu_f \Gamma}{g\rho_f(\rho_f - \rho_g)} \right)^{1/3} \qquad 3.1\text{-}1$$

where Γ is the film flowrate per unit circumference. The data were correlated such that

$$h_{exp} = f \cdot h_{ref}\,; \qquad h_{ref} = k_f/\delta_1 \qquad 3.1\text{-}2$$

where f is the correction factor (also called a degradation factor). The correction factor is divided into two parts such that $f = f_1 f_2$. The factor f_1 is the correction factor which accounts for the enhancement of heat transfer due to interfacial shear, interfacial waves and deviations from the Nusselt model. The factor f_2 is the correction factor which accounts for the effects of heat transfer degradation due to the noncondensable gas mass fraction. The Vierow and Schrock correlation then is:

$$f_1 = (1 + 2.88\text{x}10^{-5}\, Re_m^{1.18})$$

$$f_2 = (1 - C\, M_a^{b}) \qquad 3.1\text{-}3$$

where (for steam/air mixtures)

C = 10	b = 1.0	for	$M_a < 0.063$
C = 0.938	b = 0.13	for	$0.063 < M_a < 0.60$
C = 1.0	b = 0.22	for	$M_a > 0.60$

M_a is the bulk air mass fraction (air mass / total mass) at any axial location and Re_m is the local gas/steam mixture Reynolds number, $\rho UD/\mu_m$. The experimental data are shown plotted in the form of the correlation in Figure 3.1-1. The ordinate, $1-f/f_1$, is equivalent to $1-f_2$ such that when the correlation is plotted b is the slope of the curve and C fixes the position of the curve.

3.2 TRACG

The correlation used in TRACG is a modified version of the Vierow-Schrock correlation. The f_2 correlation is changed only slightly to avoid discontinuities:

$$f_2 = (1 - C M_a^b) \qquad 3.2\text{-}1$$

where (for steam/air mixtures)

C = 10	b = 1.0	for	$M_a < 0.06586$
C = 0.938	b = 0.13	for	$0.063 < M_a < 0.4911$
C = 1.0	b = 0.22	for	$M_a > 0.4911$

The f_1 term is modified as follows:

$$f_1 = 1 + 2.88 \times 10^{-5} Re_m^{1.18} \quad \text{for } Re_f \le 1000$$

$$f_1 = 1 \quad \text{for } Re_f > 2000 \qquad 3.2\text{-}2$$

$$\text{also } \delta_1 = 32.3\left(\frac{\nu_f}{\rho_f g \Gamma}\right)^{1/3} \quad \text{for } Re_f > 2000 \qquad 3.2\text{-}3$$

linear interpolation between Re_{film} of 1000 and 2000

additional restriction of $f_1 \leq 3$

where in this case $Re_f = 4\Gamma/\mu_f$

Because the f_1 correlation of Vierow and Schrock exceeds a value of 3 (near Re_m = 12,500), the TRACG correlation generally predicts lower heat transfer coefficients in the high heat transfer region near the tube inlet.

3.3 Siddique

Siddique correlated his data in the form:

$$Nu(x) = \frac{h(x)D_i}{k_m} = 6.123\,\mathrm{Re}_m^{0.223}\left(\frac{M_{a,w} - M_{a,b}}{M_{a,w}}\right)^{1.144} Ja^{-1.253} \quad 3.3\text{-}1$$

where $M_{a,w}$ is the mass fraction of air at the wall (or interface), $M_{a,b}$ is the bulk mass fraction of air, and $Ja = [Cp_{mixture}(T_b - T_w)]/h_{fg}$. The correlated data are shown in Figure 3.3-1. The MIT correlation assumes that the condensate thermal resistance is a negligible compared with the gas side resistance. This requires that the interface temperature equal the wall temperature which then allows $M_{a,w}$ to be calculated. It has been shown that this is not true for all conditions.

3.4 Ogg

Ogg [1991] correlated his data in a similar manner as did Vierow and Schrock. The f_1 correlation was obtained from pure steam data. Knowing f_1, the f_2 correlation was derived from air/steam data. His correlation is:

$$f_1 = 1 + 0.0012\,\mathrm{Re}_m^{0.7}$$

3.4-1

$$f_2 = 1 - C\,M_a^{b}$$

where

$C = 1.165$	$b = 0.26$	for	$M_a < 0.3$
$C = 0.905$	$b = 0.05$	for	$0.3 < M_a < 0.9$
$C = 1.0$	$b = 1.0$	for	$M_a > 0.9$

A comparison of the Ogg correlation with the Vierow-Schrock correlation is shown in Figures 3.4-1 and 3.4-2. The f_2 comparison shows that the two correlations are in reasonable agreement on the issue of the degradation due to the presence of noncondensable gas. The comparison of f_1 correlations show that Vierow-Schrock predicts a significantly higher amount of shear enhancement than the Ogg correlation does.

The helium/steam data were correlated also making use of the f_1 correlation:

$$f_2 = 1 - CM_a^b \qquad 3.4\text{-}1$$

where

$C = 1.59$	$b = 0.29$	for	$M_a < 0.11$
$C = 0.865$	$b = 0.014$	for	$0.11 < M_a < 0.86$
$C = 1.0$	$b = 1.0$	for	$M_a > 0.86$

M_a is the Helium mass fraction in this case.

3.5 Vial

Under the direction of Professor Schrock, Eric Vial [1993] developed a correlation from the combined databases of Vierow, Siddique, and Ogg. His effort involved only the development of a correlation and did not involve any additional experimental work. Each of the databases had certain data points excluded from the combined database.

Vierow:

- only the runs without the "temperature inversion" were used

- at the inlet of the tube $0.0103 < M_a < 0.148$
  $7138 < Re_m < 26300$

Siddique:

- the data for the first 41 cm were excluded

- at 41 cm from the inlet $0.131 < M_a < 0.525$
  $1283 < Re_m < 19905$

Ogg:

- only the data for the points located downstream of the temperature inversion region are taken into account; namely beyond the first 45 cm

- at 45 cm from the inlet $0.012 < M_a < 0.407$
  $3247 < Re_m < 39560$

Vial's correlation was of a similar form as Vierow & Schrock and also Ogg. The correlation is:

$$f_1 = 1 + 1.2\times10^{-8}\, Re_m^2 \quad \text{for } Re_m < 7000 \qquad 3.5\text{-}1$$
$$f_1 = 0.76728 + 1.06543\times10^{-4}\, Re_m \quad \text{for } Re_m > 7000$$

$$f_2 = 1 - C\, M_a^b$$

where

$C = 1.0846$	$b = 0.2344$	for	$M_a < 0.4$
$C = 0.9562$	$b = 0.0969$	for	$0.4 < M_a < 0.9$
$C = 1.0$	$b = 0.5229$	for	$M_a > 0.9$

The standard deviation is defined:

$$s = \left[\frac{\sum_{1}^{N} \left(\frac{f_{exp} - f_{Vial}}{f_{Vial}} \right)^2}{N-1} \right]^{\frac{1}{2}} \quad ; \text{N = number of points} \qquad 3.5\text{-}2$$

s = 0.3826 for the Vierow data set

s = 0.4854 for the Siddique data set

s = 0.4647 for the Ogg data set

s = 0.4613 for the combined data set

The data sets are plotted along with the new correlation in Figures 3.5-1 and 3.5-2.

3.6 Kuhn

From the results of Kuhn, UCB decided that a different form of the f_1 correlation was required. The Kuhn pure steam data were not well correlated by the old form of the f_1 correlation which was only a function of mixture Reynolds number. The new f_1 is now a combination of the heat transfer enhancement due to interfacial shear and other factors.

$$f_1 = f_{1_{shear}} \cdot f_{1_{other}} \qquad 3.6\text{-}1$$

where $f_{1_{other}}$ is a function of film Reynolds number

$$f_{1_{other}} = \phi(\mathrm{Re}_f) \qquad 3.6\text{-}2$$

The $f_{1_{shear}}$ factor is the theoretical approximation derived from smooth interface laminar film theory with interfacial shear. The $f_{1_{other}}$ factor accounts for other influences such as interfacial disturbances, deviations from linear temperature profiles, and temperature

dependent properties, etc. The f_2 correlation remains in the same form as Vierow-Schrock, Ogg, and Vial. The complete data reduction of Kuhn is given as follows:

A. Experimental heat transfer coefficient

$$h_{exp}(x) = \frac{q''_i(x)}{T_{sat}(x) - T_{Win}(x)} \qquad 3.6\text{-}3$$

B. Condensate flow rate

$$W_i(x) = \frac{\pi D_i \int_{x0}^{x} q''(x)dx}{h_{fg}} \qquad 3.6\text{-}4$$

$$\Gamma(x) = \frac{W_i(x)}{\pi D_i} \qquad 3.6\text{-}5$$

C. Calculation of two film thickness, δ_1 and δ_2

For the case without shear the film thickness is given by equation 3.1-1.

Rearranging to solve for Γ yields:

$$\Gamma = \frac{g}{\mu_f}\rho_f(\rho_f - \rho_g)\frac{\delta_1^3}{3} \qquad 3.6\text{-}6$$

With interfacial shear the predicted film thickness, δ_2, is given implicitly by:

$$\Gamma = \frac{g}{\mu_f}\rho_f(\rho_f - \rho_g)\frac{\delta_2^3}{3} + \frac{\rho_f \tau_i \delta_2^2}{2\mu_f} \qquad 3.6\text{-}7$$

where

$$\tau_i = \frac{1}{2} f_R \rho_g V_m^2 \qquad 3.6\text{-}8$$

$$f_R = 0.046 Re_m^{-0.2} \qquad 3.6\text{-}9$$

leading to the interfacial shear prediction

$$\tau_i = \frac{0.023}{\rho_g}\left(\frac{\mu_m}{D_i}\right)^2 Re_m^{1.8} \qquad 3.6\text{-}10$$

or rearranging equation 3.6-7 gives

$$\Gamma = \frac{g}{\upsilon_f}\rho_f\left(1-\frac{\rho_g}{\rho_f}\right)\frac{\delta_2^{\,3}}{3}+\frac{\tau_i\delta_2^{\,2}}{2\upsilon_f} \qquad 3.6\text{-}11$$

with $\mathrm{Re}_f = \dfrac{\Gamma}{\mu_f}$ 3.6-12

Now in dimensionless form

$$\delta_2^* = \frac{\delta_2}{L} \qquad 3.6\text{-}13$$

$$\tau_i^* = \frac{\tau_i}{g\rho_f\left(1-\dfrac{\rho_m}{\rho_f}\right)L} \qquad 3.6\text{-}13$$

with characteristic length

$$L = \left(\frac{\upsilon_f^{\,2}}{g}\right)^{1/3} \qquad 3.6\text{-}14$$

Then

$$\left(\frac{\mathrm{Re}_f}{1-\rho_m/\rho_f}\right) = \frac{\delta_2^{*3}}{3}+\frac{\tau_i^*\delta_2^{*2}}{2} \qquad 3.6\text{-}15$$

D. Determination of the correlation for f_1 factor from pure steam runs

$$f_1 = \frac{h_{exp}}{h_{\tau_i}} \qquad 3.6\text{-}16$$

$$h_{\tau_i} = \frac{k_f}{\delta_1} \qquad 3.6\text{-}17$$

assume f_1 is the combination of the heat transfer enhancement due to interfacial shear and other factors

$$f_1 = f_{1shear} \times f_{1other} \qquad 3.6\text{-}18$$

$$f_{1shear} = \frac{h_{exp}}{h_{T_2}} = \frac{h_{exp}\delta_2}{k_f} \qquad 3.6\text{-}19$$

where δ_2 is obtained numerically from solution of equation 3.6-7. Assume f_{1other} is a function of film Reynolds number

$$f_{1other} = \frac{f_1}{f_{1shear}} = \phi(Re_f) \qquad 3.6\text{-}20$$

with $\phi(Re_f) = 1 + C_1 Re_f$ 3.6-21

E Determination of the correlation for degradation factor

$$f = \frac{h_{exp}}{h_{t_1}} = f_1 \cdot f_2 \qquad 3.6\text{-}22$$

with $f_1 = \phi(Re_m, Re_f)$ 3.6-23

$$f_2 = 1 - C_2 M_o^{\ d} \qquad 3.6\text{-}24$$

Mixture Reynolds number

$$Re_m(x) = \frac{4W_m(x)}{\pi D \mu_m} \qquad 3.6\text{-}25$$

where

$$\mu_m = \frac{X_g \mu_g}{X_g + (1 - X_g)\phi_v} + \frac{(1 - X_g)\mu_v}{X_g \phi_g + (1 - X_g)} \qquad 3.6\text{-}26$$

with

$$\phi_v = \frac{\left[1 + \left(\frac{\mu_g}{\mu_v}\right)^{1/2}\left(\frac{M_v}{M_g}\right)^{1/4}\right]^2}{\left[8\left(1 + \frac{M_g}{M_v}\right)\right]^{1/2}} \qquad 3.6\text{-}27$$

and

$$\phi_g = \frac{\left[1+\left(\frac{\mu_v}{\mu_g}\right)^{1/2}\left(\frac{M_g}{M_v}\right)^{1/4}\right]^2}{\left[8\left(1+\frac{M_v}{M_g}\right)\right]^{1/2}} \qquad 3.6\text{-}28$$

The correlation of Kuhn is:

$$f = f_1 f_2 \qquad 3.6\text{-}22$$

$$f_1 = f_{1_{shear}} \cdot f_{1_{other}}$$

$f_{1_{shear}}$ determined from equation 3.6-19

$$f_{1_{other}} = 1 + 7.32\text{x}10^{-4}\text{Re}_f \qquad 3.6\text{-}24$$

$$f_2 = (1 - C\,M_a{}^b)$$

where

C = 2.601	b = 0.708	for	$M_a < 0.1$
C = 1.0	b = 0.292	for	$M_a > 0.1$

For helium the f_1 correlation remains the same as the air correlation. The f_2 correlation for helium is:

$$f_2 = 1 - C\,M_a{}^b$$

where

$C = 35.81$	$b = 1.074$	for	$M_a < 0.01$
$C = 2.09$	$b = 0.457$	for	$0.01 < M_a < 0.1$
$C = 1.0$	$b = 0.137$	for	$M_a > 0.1$

The $f_{\_}$ correlation is plotted versus film Reynolds number along with the pure steam data in Figure 3.6-1. The correlation (and plot) were created from 33 pure steam runs. The standard deviation of the data from the f_1 correlation is 7.4%.

Figure 3.6-2 shows the f_2 correlation (plotted as $1\text{-}f_2$) and the 68 steam-air cases from which it was calculated. The standard deviations for the data for the two different regions are shown on the plot. The experimental total degradation is plotted versus the degradation predicted by the Kuhn correlation in Figure 3.6-3. The data spread is small as evidenced by the 18% standard deviation. This is considerably smaller than the standard deviations for the Vial correlation. The standard deviation of Ogg's data with his correlation was 27%. Figures 3.6-4 and 3.6-5 show the corresponding graphs for the steam-helium cases. The standard deviation is shown in Figure 3.6-5 to be 13%.

A comparison of the heat transfer coefficient predicted by the Kuhn correlation is made with the heat transfer coefficient predicted by Vierow and Schrock (Tsukuba) for the Kuhn experimental conditions in Figure 3.6-6. The crosses represent predictions of the correlations for the conditions of the 68 steam-air runs. Note that the Kuhn correlation predicts a consistently lower heat transfer coefficient than does Vierow-Schrock. The f_2 correlation of Vierow and Schrock and the f_2 correlation of Kuhn are plotted versus air mass fraction in Figure 3.6-7. The plot shows that less degradation caused by the presence of air is predicted by Kuhn than is predicted by Vierow and Schrock. Because the Vierow-Schrock correlation was not applied directly in TRACG it is also useful to compare the TRACG correlation results with Kuhn. Figure 3.6-8 compares the Kuhn et al. correlation with the Vierow-Schrock correlation with the restriction that $f_1 \leq 3$. The additional changes for $4\Gamma/\mu > 1000$ were not included. Most of the data are for values of $4\Gamma/\mu$ less than 1000. The restriction on f_1 brings the two correlations are in better agreement, though Kuhn still predicts lower heat transfer coefficients. The impact of the different predictions will be discussed in Section 4.1.

Similar comparisons of Kuhn with Ogg and Vial are shown in Figures 3.6-9 and 3.6-10, respectively. The Kuhn correlation also predicts lower heat transfer coefficients

than these two correlations predict. Finally a comparison was made against a general correlation for steam condensation inside of tubes found in Chen et. al. [1987]. Though the applicability of this correlation to the present conditions may be questioned, the comparison is made in order to satisfy the desire to compare the Kuhn correlation with any in the existing literature. Figure 3.6-11 shows that Kuhn also predicts a lower heat transfer coefficient than Chen predicts.

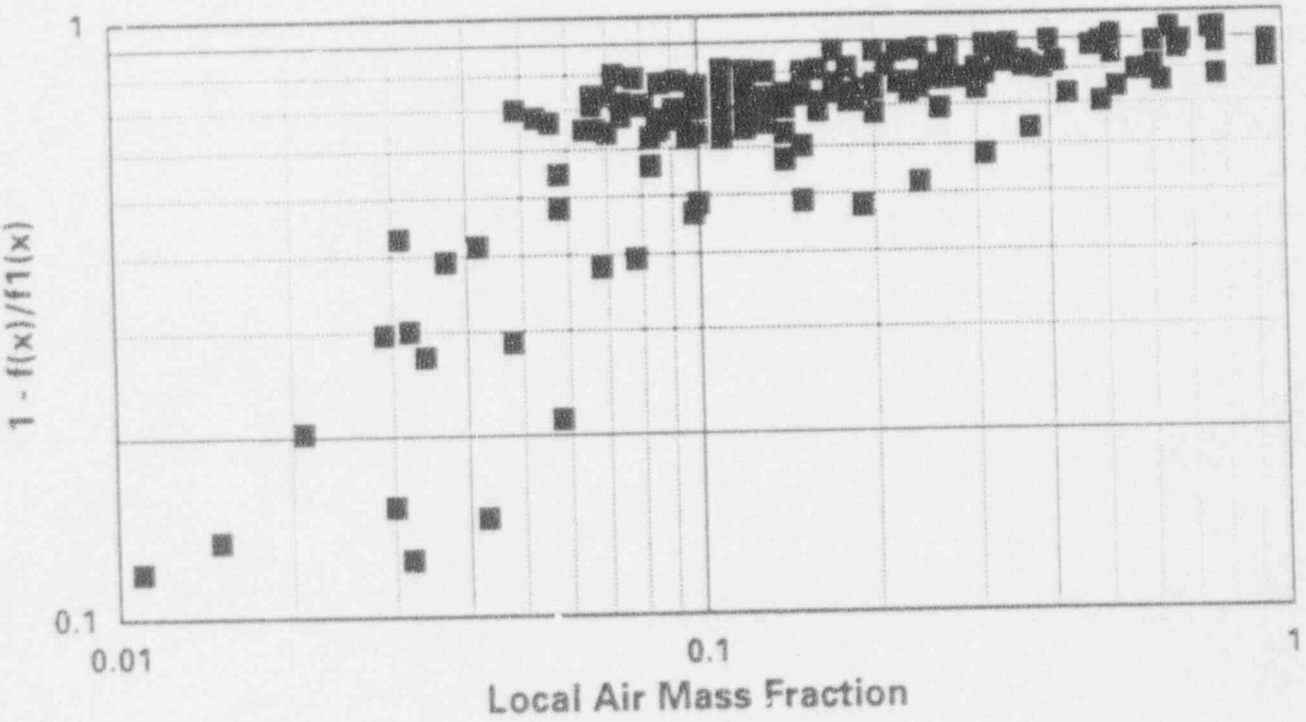

Figure 3.1-1: Data plotted in the form of the Vierow-Schrock [1991] correlation. The factor $1-f/f_1$ is plotted versus local air mass fraction. Used with permission.

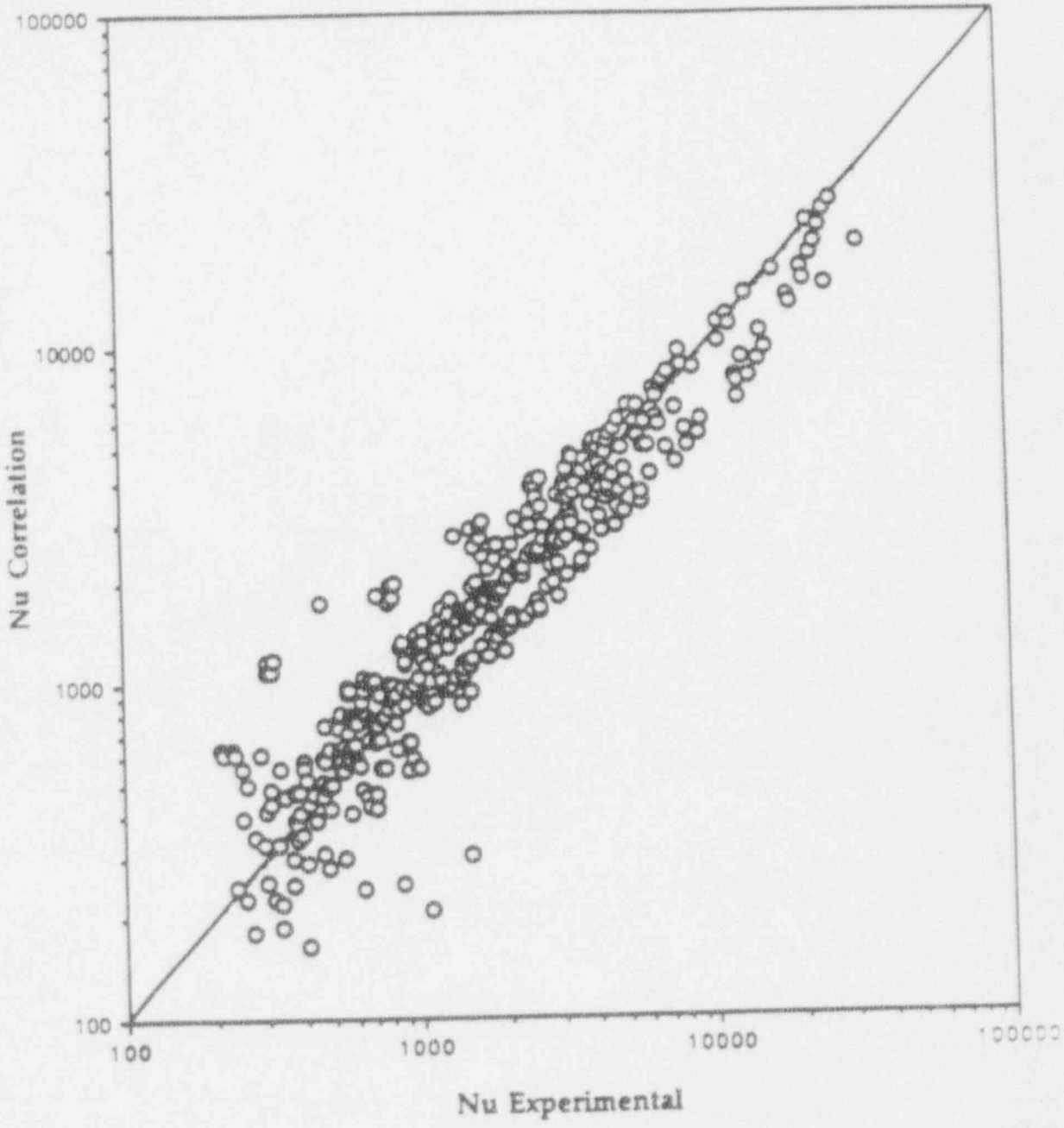

Figure 3.3-1: A comparison of the air/steam Nusselt numbers produced by the Siddique [1992] correlation versus the experimental Nusselt numbers. Used with permission.

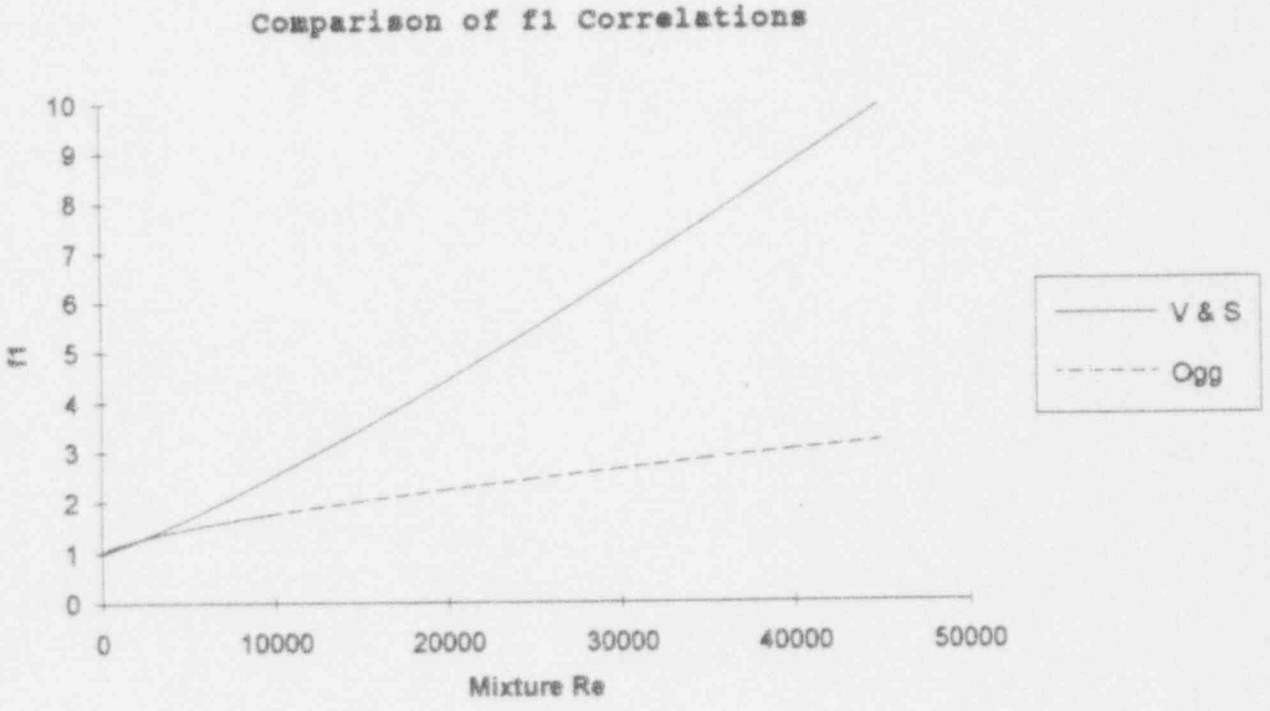

Figure 3.4-1. A comparison of the f_1 correlations of Vierow and Schrock [1991] and Ogg [1991] plotted against mixture Reynolds number.

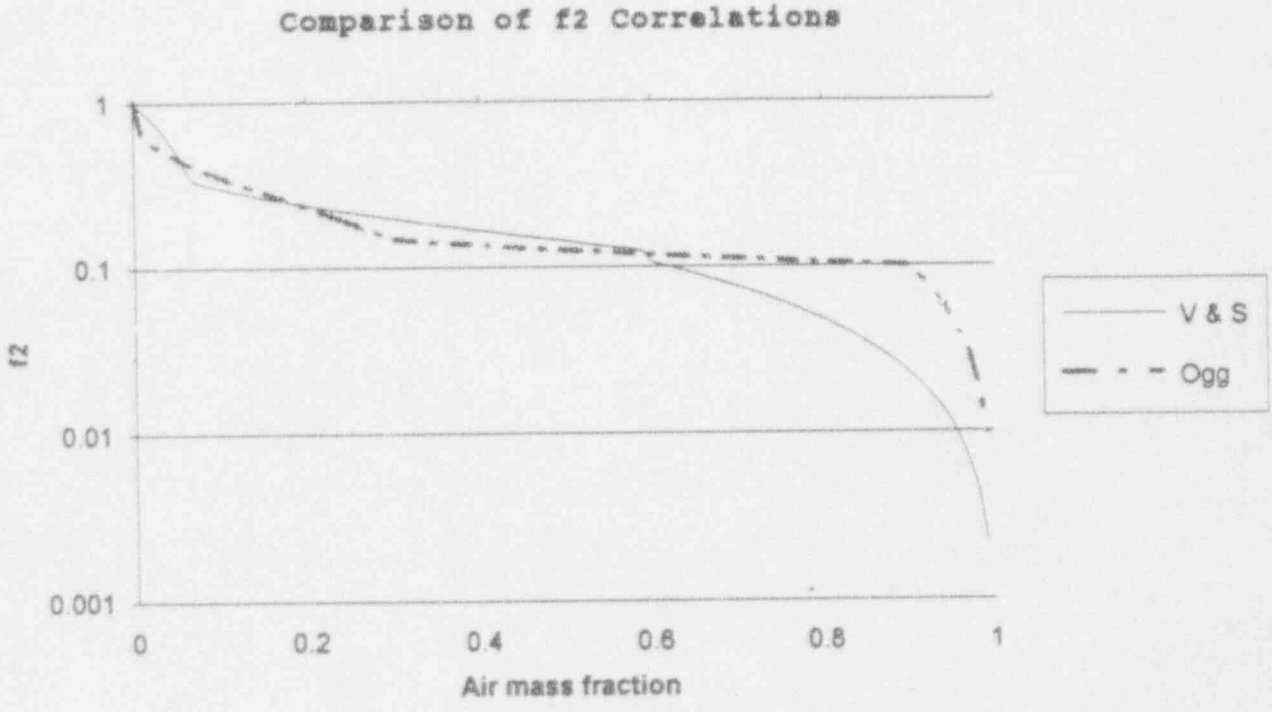

Figure 3.4-2: Comparison of the f_2 correlation of Vierow and Schrock [1991] and Ogg plotted against air mass fraction.

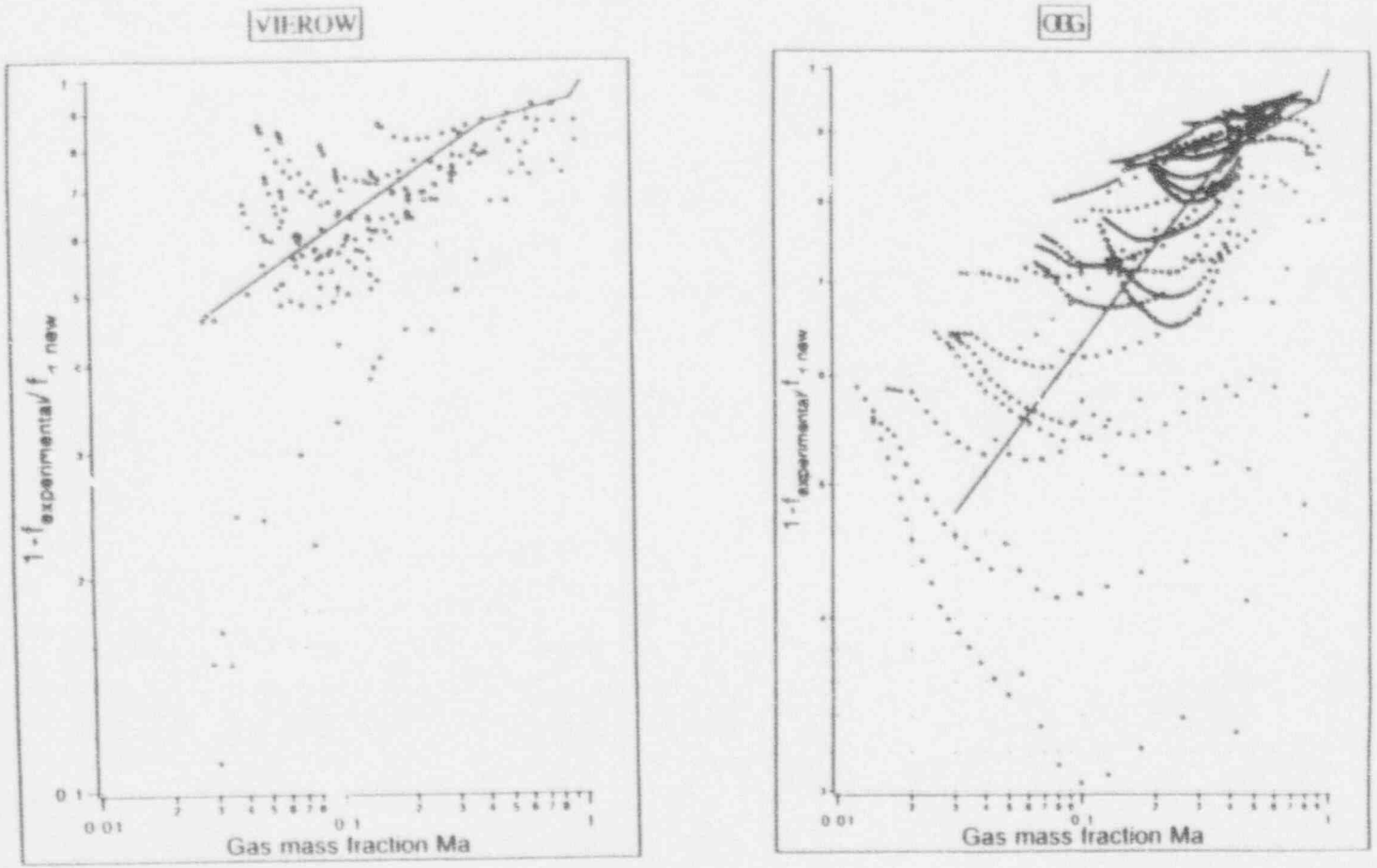

Figure 3.5-1: Plots of the Vierow [1990] and Ogg [1991] data plotted along with the Vial correlation.

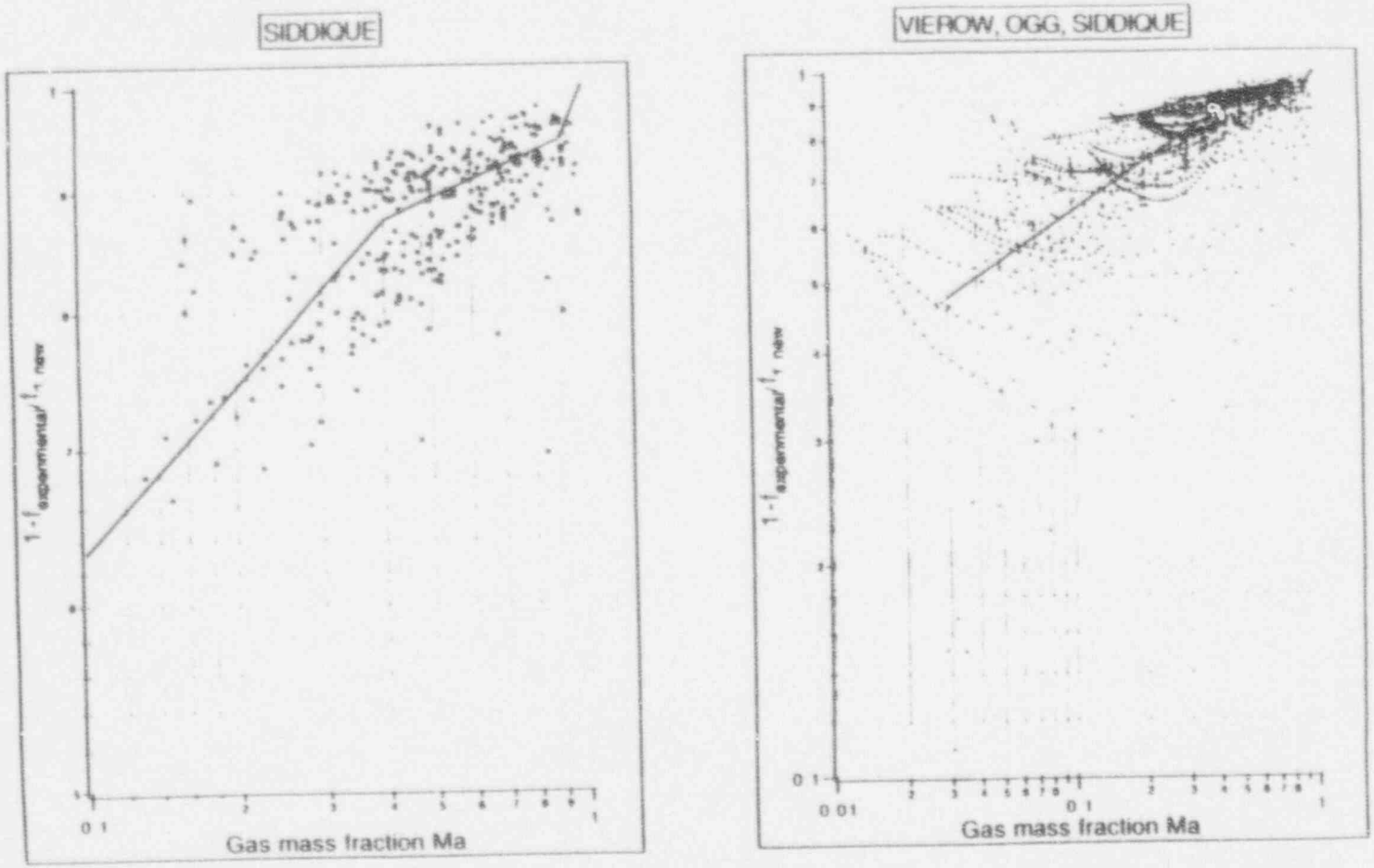

Figure 3.5-2: Plots of both the Siddique [1992] data and the combined data base along with the Vial correlation.

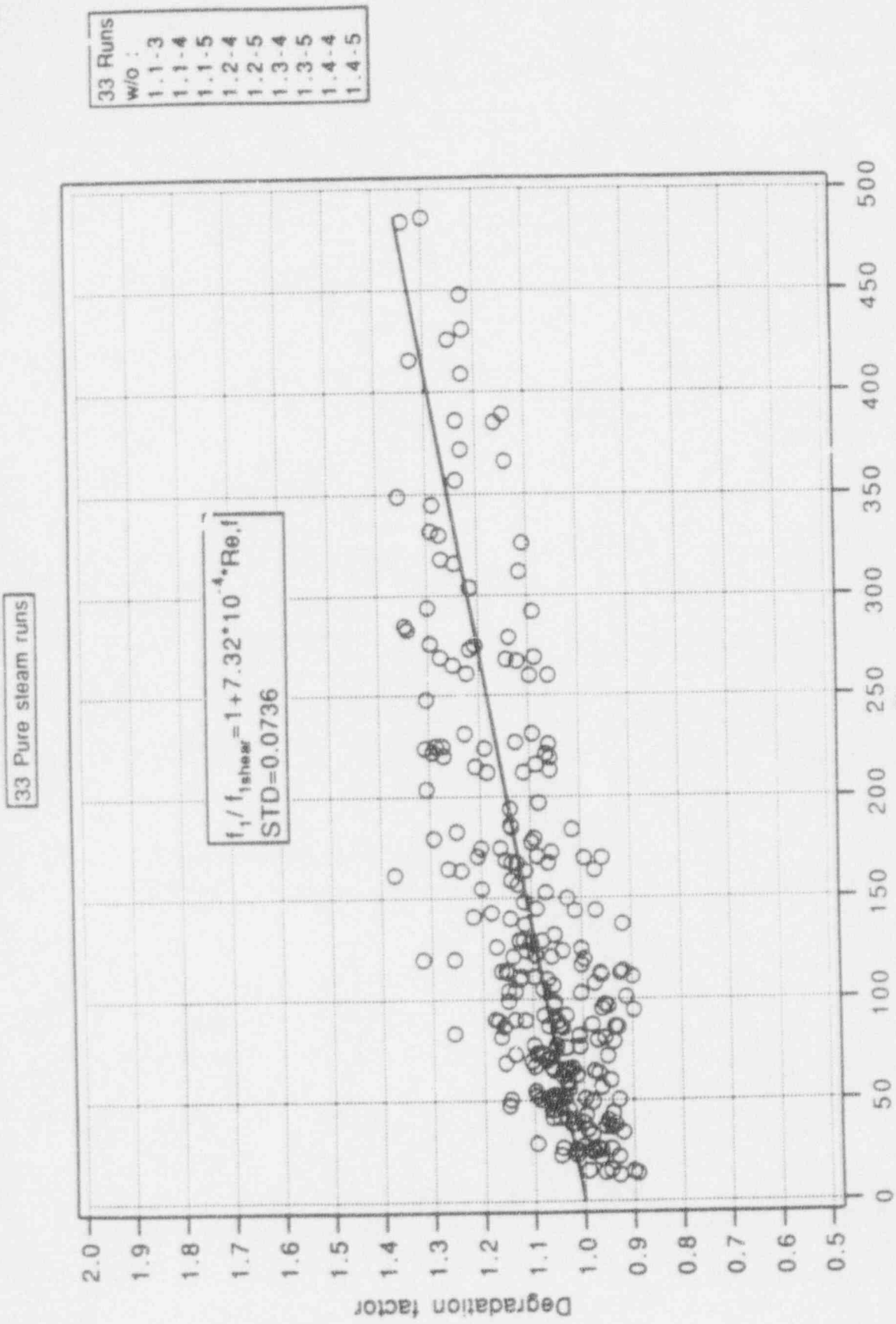

Figure 3.6-1. Plots of f_1/f_{1shear} versus film Reynolds number for the pure steam data of Kuhn et al [1993].

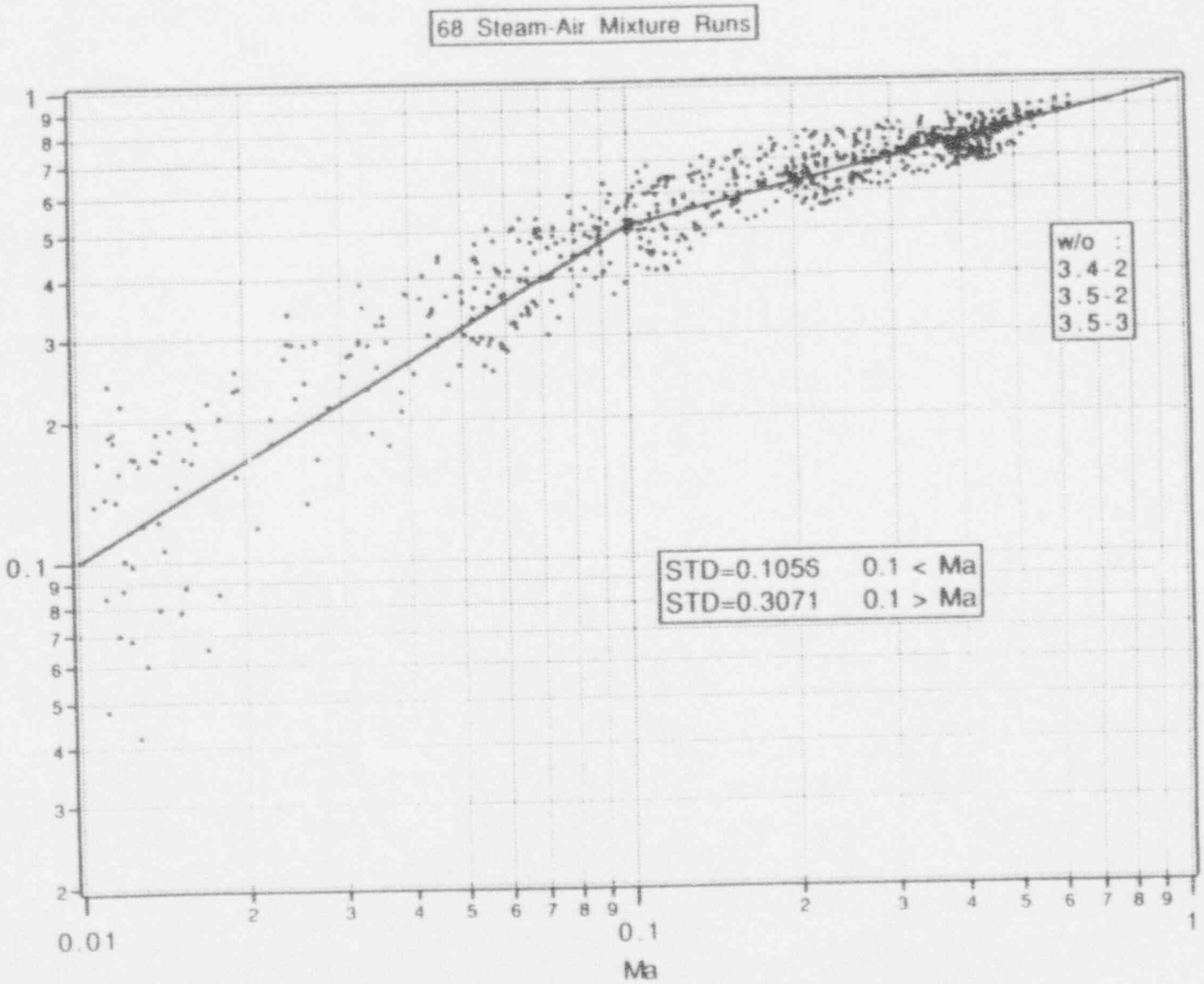

Figure 3.6-2: Plot of the Kuhn steam/air data along with the Kuhn et al. [1993] correlation for 68 steam/air runs. The ordinate is equivalent to 1- f_2.

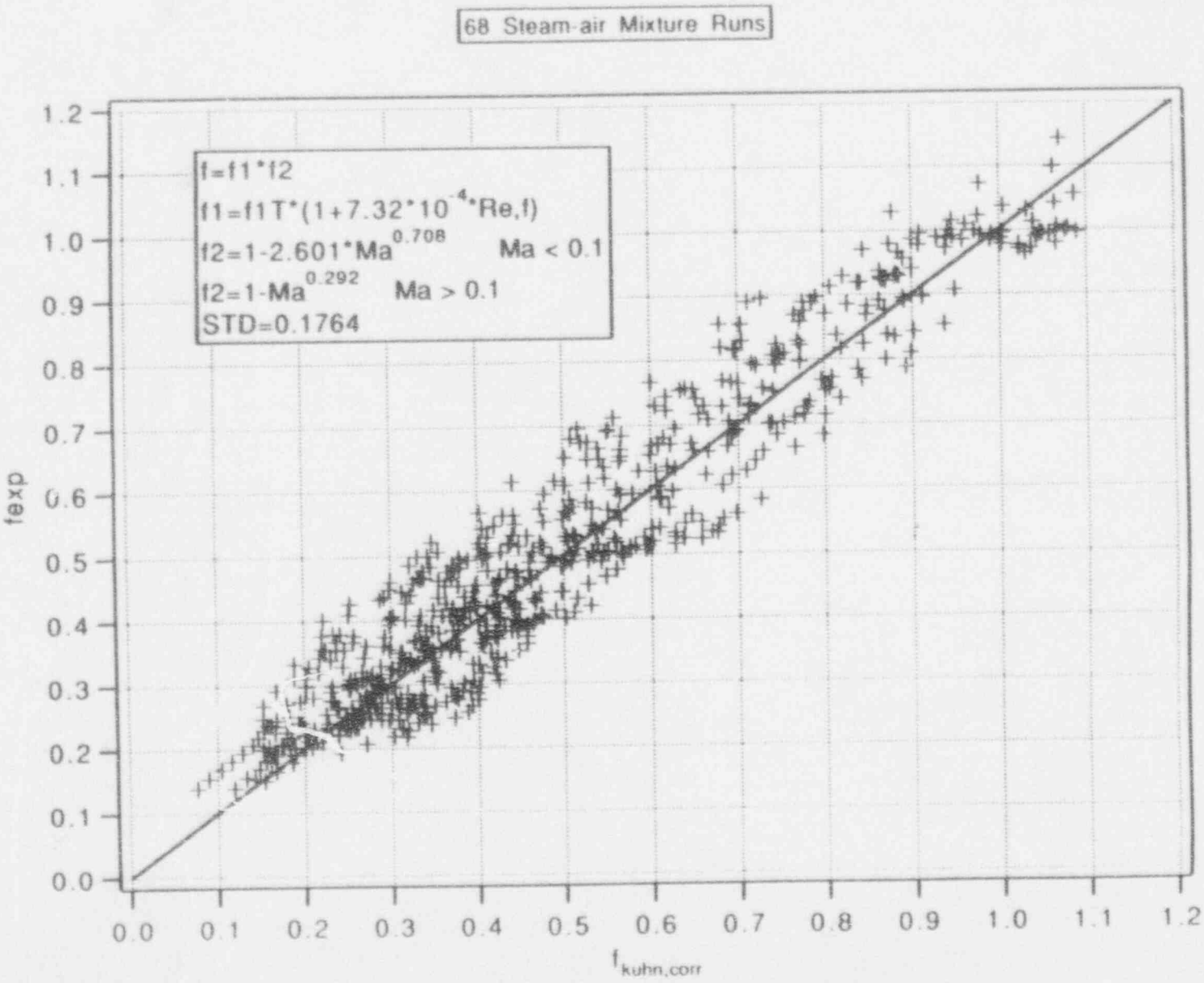

Figure 3.6-3: Plot of the steam/air mixture experimental degradation factor versus the degradation factor predicted by the Kuhn et al. [1993] correlation.

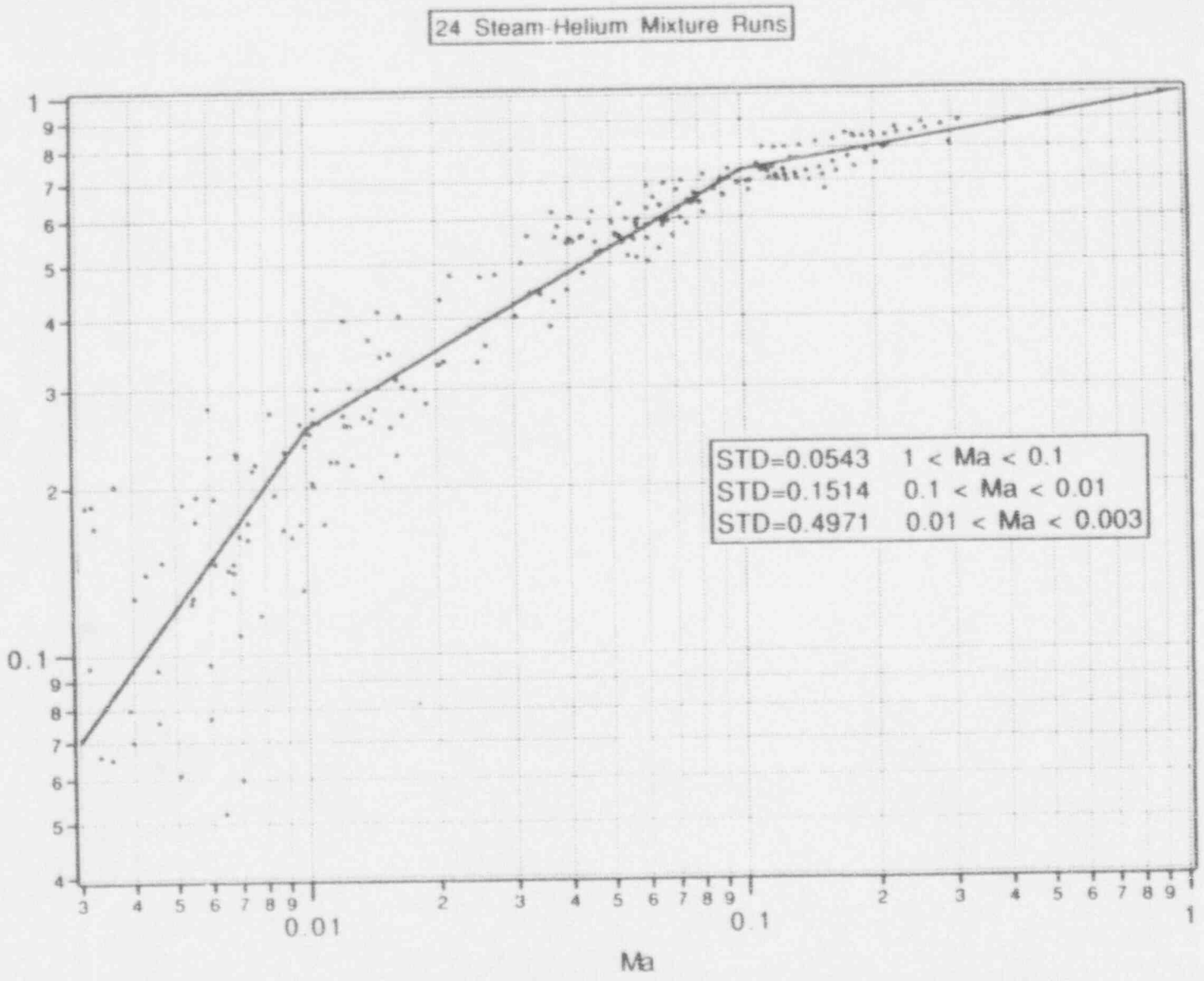

Figure 3.6-4. Plot of the Kuhn steam/helium data along with the Kuhn et al. [1993] helium correlation for 24 steam/air runs. The ordinate is equivalent to 1-f_2.

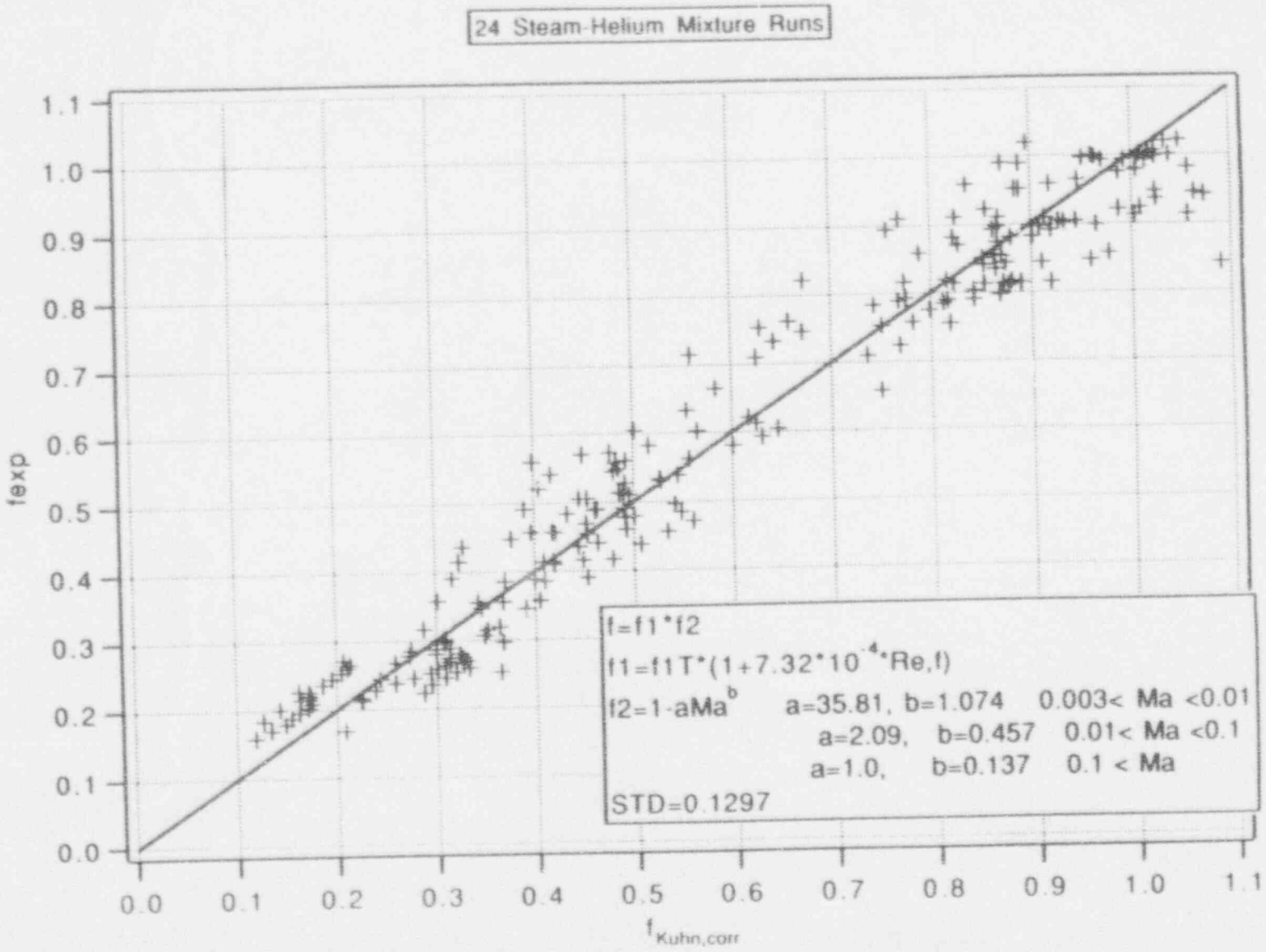

Figure 3.6-5: Plot of the steam/helium mixture experimental degradation factor versus the degradation factor predicted by the Kuhn et al. [1993] helium correlation

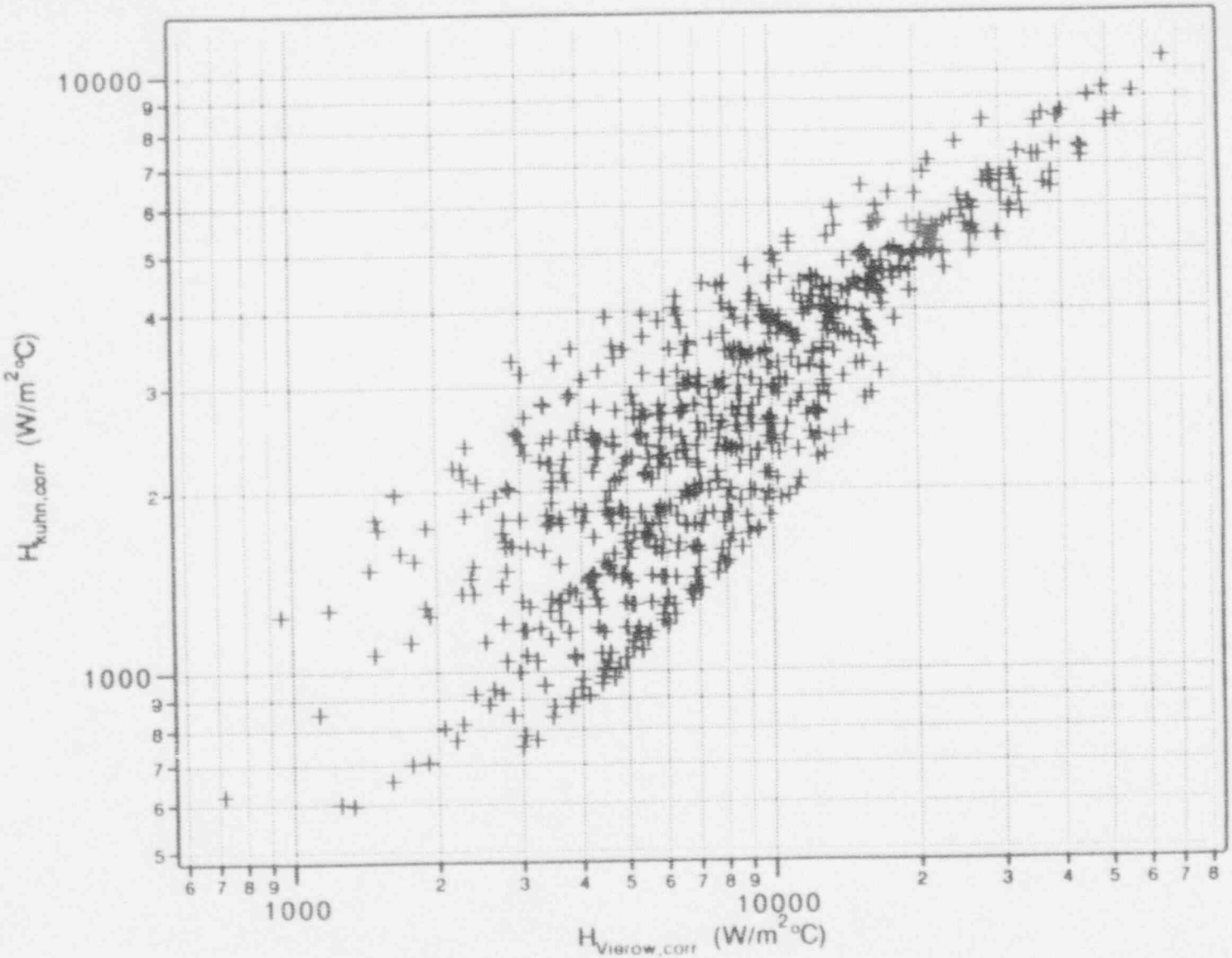

Figure 3.6-6 Plot of the heat transfer coefficient predicted by the Kuhn et al. [1993] steam/air correlation versus the heat transfer coefficient predicted by the Vierow and Schrock correlation

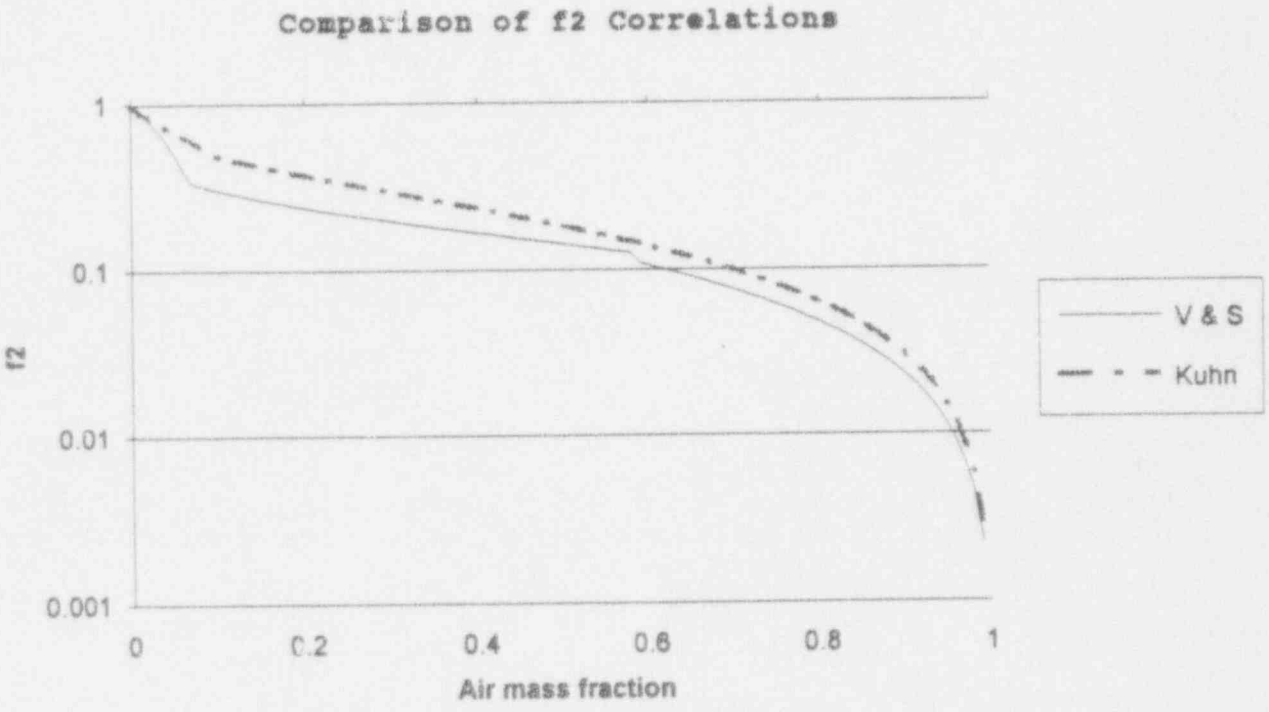

Figure 3.6-7: Comparison of the f_2 correlation of Vierow and Schrock and Kuhn et al. [1993] plotted against air mass fraction.

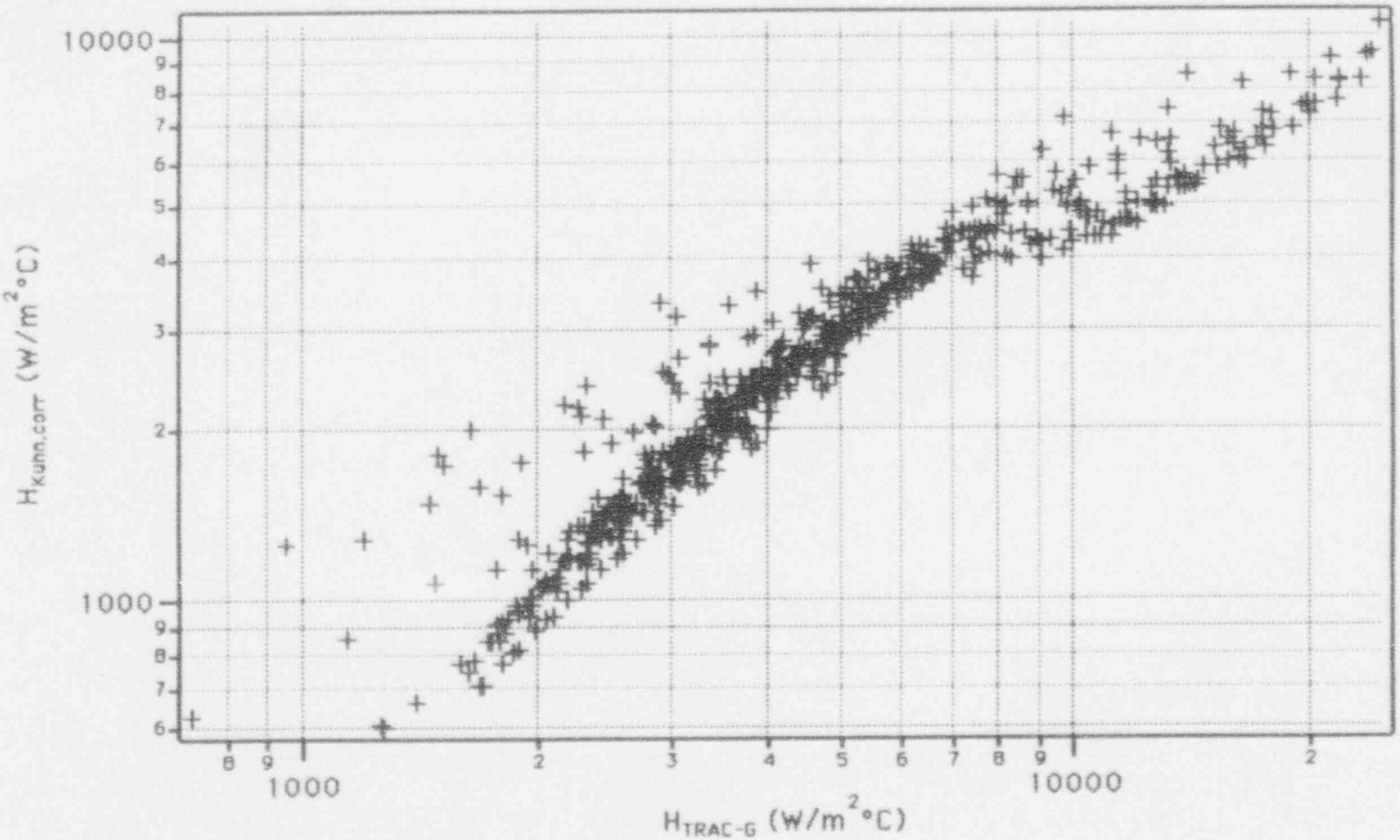

Figure 3.6-8. Plot of the heat transfer coefficient predicted by the Kuhn et al. [1993] steam/air correlation versus the heat transfer coefficient predicted by the correlation currently in TRACG.

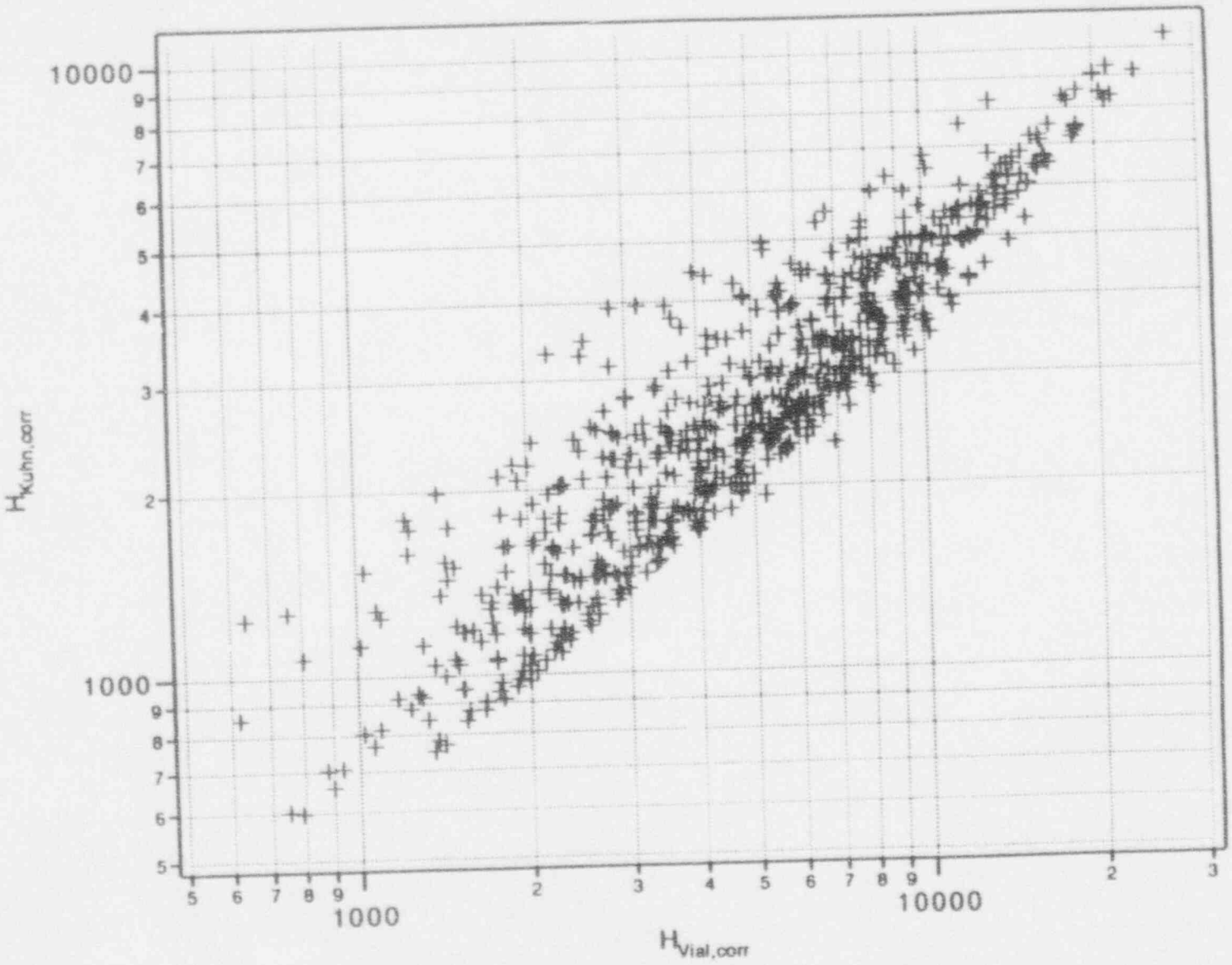

Figure 3.6-9 Plot of the heat transfer coefficient predicted by the Kuhn et al. [1993] steam/air correlation versus the heat transfer coefficient predicted by the Vial correlation.

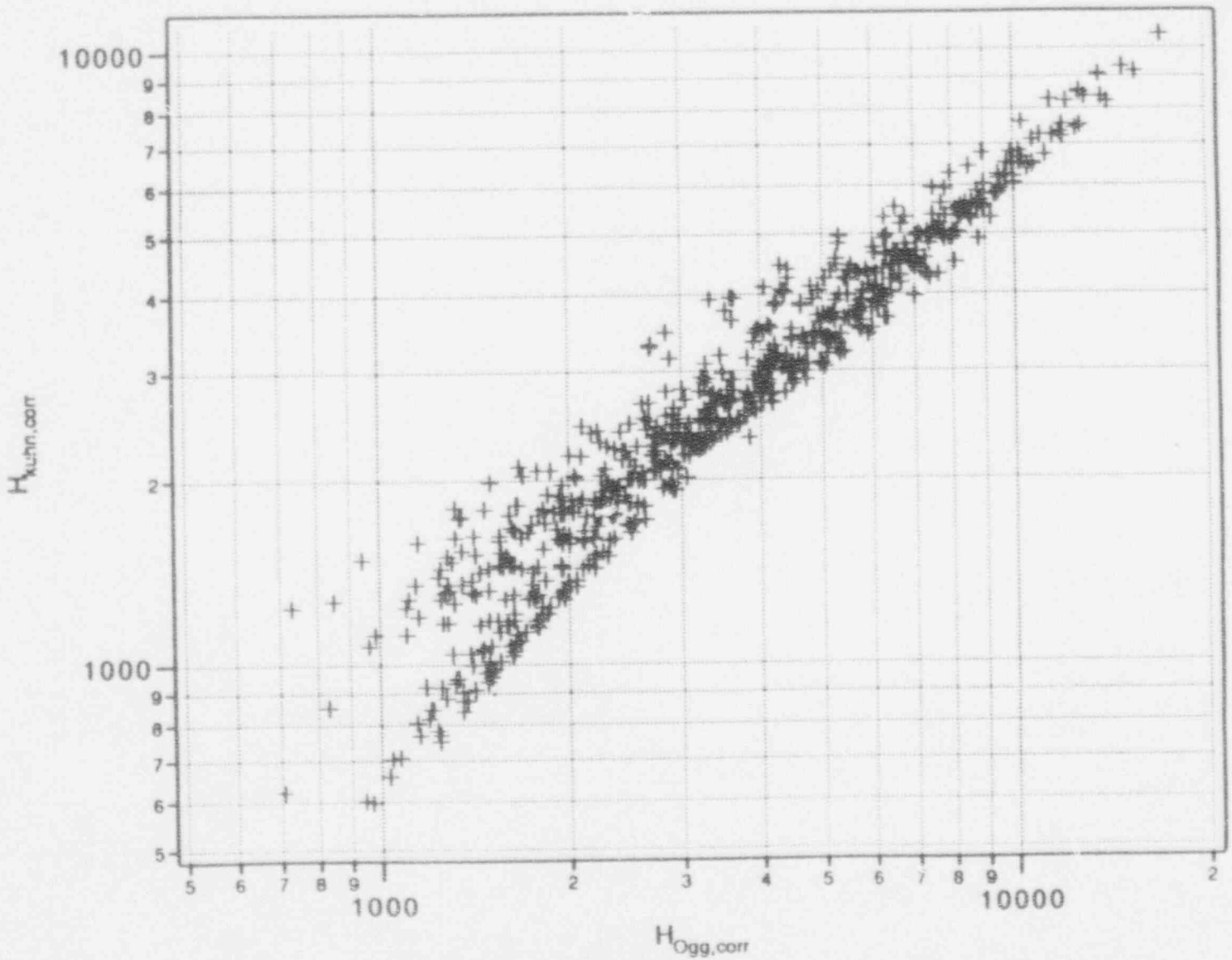

Figure 3.6-10 Plot of the heat transfer coefficient predicted by the Kuhn et al. [1993] steam/air correlation versus the heat transfer coefficient predicted by the Ogg correlation.

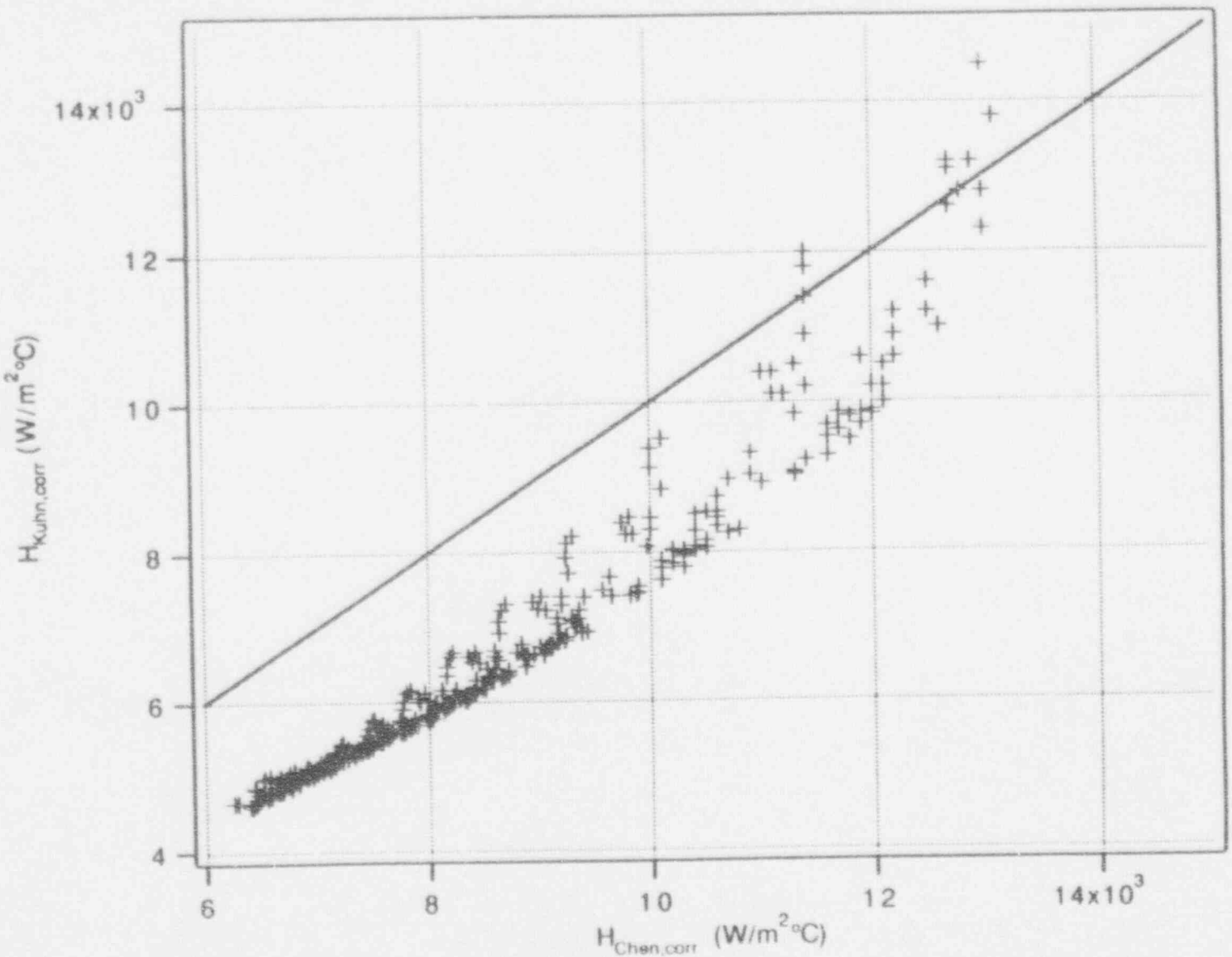

Figure 3.6-11 Plot of the heat transfer coefficient predicted by the Kuhn et al. [1993] steam/air correlation versus the heat transfer coefficient predicted by the Chen [1987] correlation

4. DISCUSSION

4.1 Impact on TRACG Analysis

The results presented in the previous section show that the correlation in TRACG predicts a higher heat transfer coefficient (htc) than the Kuhn correlation. The potential impact of this result on the post-LOCA containment performance analysis should be evaluated by considering the overall thermal resistance from the steam inside the tube to the pool outside. Typically, the current TRACG correlation predicts that the inside resistance is about 25% of the total. From the results shown in Figure 3.6-8, the Kuhn correlation would raise the inside resistance to about 35% of the total resistance. The effect of this change is equivalent to a 20% reduction in the condenser heat transfer area. Kim et al. [1993], submitted to the NRC in February 1993, presented the results of a TRACG sensitivity study in which the PCCS heat transfer area was reduced by 33%. It was shown that the effect was to raise the containment pressure by 17 kPa (2.5 psi). For a 20% reduction in heat transfer area the expected effect would be a 10 kPa (1.5psi) increase. In the same reference, it was stated that improvements in the containment model had resulted in a decrease in the peak containment pressure relative to that presented in GENE [1992], submitted to the NRC in August 1992. The magnitude of this decrease is larger than the expected increase from the use of the Kuhn correlation. Thus, the peak pressure predicted with the current model and the Kuhn correlation will be less than the value presented in SSAR.

An additional indication of the relatively small sensitivity of predicted condenser performance to a reduction in the inside htc is provided by the comparison of TRACG predictions with GIRAFFE data presented in Andersen [1993], also submitted to the NRC in February, 1993. Those comparisons, made with the Tsukuba correlation, show satisfactory agreement of the TRACG predictions with both the Step 1 steady-state condenser performance, and Step 3 integral system test results.

4.2 Applicability of Kuhn Correlation to IC Tubes

The applicability of the Kuhn correlation to high pressure pure steam environments will be addressed initially here in this report and also in Schrock et al. [1994] and Usry [1994]. The IC tubes operate at pressures near 70 atmospheres. The maximum pressure tested in the university tests is 5 atmospheres. The data of Kuhn are well correlated over

the range of 1 to 5 atmospheres. Because the IC tubes will generally experience minimal degradation due the presence of noncondensable gases, the f_2 correlation is not critical. The $f_{i_{shear}}$ correlation, on the other hand, is relevant and includes first order effects of pressure in equation 3.6-10 in the $0.023/\rho_g$ term. As the pressure increases the shear enhancement is reduced in a linear manner. The sensitivity of the TRACG analysis of the IC performance is expected to be very small because the limiting resistance is not the gas-side resistance. Because the ICs contain only small amounts of noncondensable gases and have thicker tubes, the gas-side resistance will be an even smaller part of the overall resistance in the IC's than it is in the TRACG PCCS performance analysis. This will be addressed further in the final report on the university single tube condensation tests (Usry [1994]).

5.0 SUMMARY

When this experimental program began, there was no known local heat transfer data or correlation for forced flow steam condensation inside of tubes in the presence of noncondensables. At two Universities, five experiments using four different test rigs have now investigated this phenomenon. Lessons learned from each of them were applied to subsequent tests, such that the final test at UC Berkeley has produced a correlated data set with a standard deviation of only 18%. The effect of the most recent data on the SBWR post-LOCA containment analysis has been evaluated by comparison with a previous sensitivity study on PCCS heat transfer area. The results indicate that the effect is small and bounded by the peak containment pressure presented in the August, 1992 SSAR. An additional GE report will document any new work at UCB and MIT completed after this report.

6.0 REFERENCES

Andersen, J. G. M. et al., 1993, TRACG Qualification, NEDE-32177P, Rev. 1, Class 3, June, 1993.

Chen, S. L., Gerner, F. M. and Tien, C. L., 1987, "General Film Condensation Correlations," Experimental Heat Transfer, Vol. 1, pp. 93-107.

GENE, 1992, SBWR Standard Safety Analysis Report, 25A5113, Rev. A, August, 1992.

Golay, M. W., 1993, phone conversation with W. R. Usry, October, 1993.

Kim, H. T., et al, 1993, Application of TRACG Model to SBWR Licensing Safety Analysis, NEDE-32178P, Class 3, February, 1993.

Kuhn, J. S. Z., Schrock, V. E., Peterson, P. F., 1993, in preparation.

Ogg, D. G., 1991, "Vertical Downflow Condensation Heat Transfer in Gas-Steam Mixtures", M.S. Thesis, U.C. Berkeley Dept. of Nuclear Engineering.

Schrock, V. E., 1993, Presentation to the NRC on the subject of the Single Tube Condensation Tests, San Jose, June 10, 1993.

Schrock, V.E., Peterson, P.F., Kuhn, J.S.Z., Yuann, R.Y., Ogg, D.G., Kageyama, T., Vial, E., and Vierow, K.M., 1994, Final Report of the UCB Study of Condensation Phenomenon in the Presence of Noncondensables, in preparation.

Siddique, M., 1992, "The Effects of Noncondensable Gases on Steam Condensation under Forced Convection Conditions", Doctor of Philosophy Dissertation, Massachusetts Institute of Technology.

Usry, W. R., 1994, Single Tube Condensation Tests, Revision 1.

Vial, E., and Schrock, V. E., 1993, "A Correlation Based on the Combined UCB and MIT Data Sets for Condensation Inside Tubes with Noncondensable Gas", UCB-NE-4193, April 1993.

Vierow, K. M., 1990, "Behavior of Steam-Air Systems Condensing in Cocurrent Vertical Downflow", M.S. Thesis, U.C. Berkeley Dept. of Nuclear Engineering.

Vierow, K. M. and Schrock, V. E., 1991, "Condensation in a Natural Circulation Loop with Noncondensable Gases, Part I and II, Proceedings of the International Conference on Multiphase Flows, Tsukuba, Japan.

Vierow, K. M., J. R. Fitch, F. E. Cooke, 1992, "Analysis of SBWR Passive Containment Cooling Following a LOCA", International Conference on the Design and Safety of Advanced Nuclear Power Plants, Tokyo, Japan.

Wilkins, D. R., S. A. Hucik, R. C. Berglund, R. J. McCandless, 1992, "GE Advanced Boiling Water Reactors for the 1990's and Beyond", International Conference on the Design and Safety of Advanced Nuclear Power Plants, Tokyo, Japan.

APPENDIX

(Kuhn data used for pressure drop calculation)

Run 1.1-1

Ws = 60.2 Kg/hr
Wj = .0 Kg/hr
Wcw = 999.8 Kg/hr

Pinlet = 116.1 KPa
Tinlet = 138.8 °C

Tc,i = 31.5 °C
Tc,o = 52.0 °C

Tc-fit = D
Point =11
STD = .19 °C

Length cm	Ta °C	Tcw °C	Tc-fit °C	Two °C	Tw °C	Twi °C	Tsat °C	Tcl °C	dTcw/dX °C/m	q" W/m^2	Wcond Kg/hr	Wsteam Kg/hr	Film-dx m
17.0	47.5	51.4	51.0	93.0	94.1	99.0	103.9	136.8	7.041	.548E+05	2.17	58.03	.721E-04
30.4	46.0	50.0	50.1	92.3	93.3	98.2	103.9	136.5	6.945	.540E+05	3.85	56.35	.874E-04
44.6	45.1	49.0	49.1	91.1	92.1	96.9	103.9	136.0	6.845	.533E+05	5.60	54.60	.992E-04
61.5	44.0	48.1	47.9	91.3	92.3	97.0	103.9	135.4	6.728	.523E+05	7.66	52.54	.110E-03
79.8	42.8	46.9	46.7	90.6	91.6	96.2	103.9	134.7	6.604	.514E+05	9.84	50.36	.120E-03
99.6	41.1	45.3	45.4	89.4	90.4	9[illegible] 9	103.9	133.9	6.472	.503E+05	12.15	48.05	.129E-03
121.3	39.8	44.0	44.0	88.9	89.9	94.4	103.9	133.1	6.330	.492E+05	14.63	45.57	.137E-03
145.1	38.4	42.7	42.5	88.7	89.6	93.9	103.9	132.5	6.178	.481E+05	17.28	42.92	.145E-03
171.5	36.8	40.9	40.9	84.9	85.8	90.1	103.9	131.5	6.014	.468E+05	20.11	40.09	.154E-03
201.5	34.8	38.9	39.1	82.6	83.5	87.6	103.9	130.6	5.833	.454E+05	23.24	36.96	.162E-03

Length cm	Re,f	X Gas mass %	Ω Gas mole %	P steam KPa	P gas KPa	μ(mix) Kg/m^2	Re(mix)	Htheor W/m^2.°C	Hexp W/m^2.°C	Dfactor	R(in) m^2°C/W	R(tube) m^2°C/W	R(out) m^2°C/W
17.0	.145E+02	.000	.000	116.1	.0	.122E-04	.354E+05	.946E+04	.113E+05	1.199	.882E-04	.109E-03	.821E-03
30.4	.256E+02	.000	.000	116.1	.0	.122E-04	.344E+05	.780E+04	.949E+04	1.217	.105E-03	.109E-03	.815E-03
44.6	.371E+02	.000	.000	116.1	.0	.122E-04	.333E+05	.687E+04	.766E+04	1.115	.131E-03	.109E-03	.843E-03
61.5	.507E+02	.000	.000	116.1	.0	.122E-04	.320E+05	.619E+04	.765E+04	1.237	.131E-03	.109E-03	.886E-03
79.8	.649E+02	.000	.000	116.1	.0	.122E-04	.307E+05	.568E+04	.674E+04	1.186	.148E-03	.110E-03	.914E-03
99.6	.795E+02	.000	.000	116.1	.0	.122E-04	.293E+05	.529E+04	.565E+04	1.069	.177E-03	.110E-03	.935E-03
121.3	.955E+02	.000	.000	116.1	.0	.122E-04	.278E+05	.496E+04	.518E+04	1.044	.193E-03	.110E-03	.976E-03
145.1	.113E+03	.000	.000	116.1	.0	.122E-04	.262E+05	.469E+04	.485E+04	1.034	.206E-03	.110E-03	.103E-02
171.5	.128E+03	.000	.000	116.1	.0	.122E-04	.244E+05	.443E+04	.339E+04	.766	.295E-03	.110E-03	.101E-02
201.5	.146E+03	.000	.000	116.1	.0	.122E-04	.225E+05	.420E+04	.280E+04	.666	.357E-03	.111E-03	.102E-02